NASA
Technical
Paper
2581

June 1986

NASA-TP-2581 19860017571

Pressure Probe and Hot-Film Probe Responses to Acoustic Excitation in Mean Flow

Tony L. Parrott and
Michael G. Jones

NASA

NASA Technical Paper 2581

1986

Pressure Probe and Hot-Film Probe Responses to Acoustic Excitation in Mean Flow

Tony L. Parrott
Langley Research Center
Hampton, Virginia

Michael G. Jones
PRC Kentron, Inc.
Hampton, Virginia

National Aeronautics and Space Administration

Scientific and Technical Information Branch

SUMMARY

An experiment was conducted to compare the relative responses of a hot-film probe and a pressure probe positioned in a flow duct carrying mean flow and progressive acoustic waves. The response of each probe was compared with that of a condenser-type microphone flush mounted in the duct wall. It was convenient to compare the hot-film probe response with that of the flush-mounted condenser microphone in terms of normalized fluctuating Reynolds number and normalized fluctuating pressure. The pressure probe response was correlated with the flush-mounted microphone response in terms of fluctuating pressure. Acoustic pressure excitation levels from 120 to 147 dB at test frequencies of 0.5 to 3.0 kHz were superimposed on mean flows with nominal centerline Mach numbers of 0.1, 0.3, and 0.5.

The response of the pressure probe was less than that of the flush-mounted microphone by not more than about 2.1 dB at the centerline Mach number of 0.5. This decreased response of the probe can likely be attributed to flow-induced impedance changes at the probe sensor orifices. The response of the hot-film probe, expressed in terms of fluctuating pressure, was greater than that of the flush-mounted microphone by as much as 6.0 dB at the two higher centerline Mach numbers. Removal of the temperature-related term in the analytical model of the hot-film response eliminated a large portion of the observed relative response discrepancy. When compared in terms of fluctuating Reynolds number, the hot-film relative response was at most 5.0 dB above that of the flush-mounted microphone at the higher centerline Mach numbers. Removal of the contribution from fluctuating temperature in the hot-film analytical model again greatly improved the agreement between the two transducer responses.

These results suggest that with careful calibration procedures, hot films can be used to estimate the acoustic contribution to fluctuating mass flux intensity in a boundary layer subjected to acoustic excitation. Thus, hot films should be capable of operation in the proximity of a surface where a larger pressure probe might cause unacceptable disturbance of the flow field. These data also indicate that the pressure probe provides a good method for accurately measuring acoustic pressure fluctuations in a flow field where the disturbance caused by a streamlined probe is acceptable.

INTRODUCTION

The measurement of coherent acoustic fields in the presence of subsonic flow with mean shear is of fundamental interest to researchers concerned with acoustic excitation of laminar boundary-layer instability waves (Tollmien-Schlichting) that may cause transition to turbulent flow. Acoustic pressure field amplitude spectra, propagation directions, and gradients are needed inputs for evaluating laminar boundary-layer receptivity to acoustic excitation. (See refs. 1, 2, and 3.) Also, according to Morkovin and Corke (ref. 1), the acoustic field at a wall acquires an acoustic vorticity sublayer because of the no-slip condition. On the other hand, Tollmien-Schlichting waves are essentially vortical. It is plausible, therefore, to look to the immediate neighborhood of the wall for a possible coupling of the driving sound

to the responding vorticity field. Thus, a complete experimental characterization of the response of a boundary layer to acoustic excitation may require both pressure and velocity-like measurements such as fluctuating mass flux or Reynolds number. In particular, Maestrello, Parikh, Bayliss, and Turkel (ref. 2) have calculated growth rates of flow disturbances over flat plates arising from controlled localized heating on the basis of fluctuating mass flux.

Past development of pressure probes for acoustic measurements in a flow environment has been largely limited to sound pressure level measurements of low-frequency broadband noise in flow duct systems. The requirements in such applications have been an improved acoustic-signal-to-flow-noise ratio and high directionality. Neise (refs. 3 and 4) has investigated slit-type probes that exhibit improved acoustic-signal-to-flow-noise ratios of more than 10 dB with sensitivity variations of less than 0.5 dB over the frequency range of 40 to 1250 Hz at flow speeds up to 40 m/s. Flow noise reduction for these probes was accomplished by connecting a microphone to one end of a long, cylindrical cavity (about 0.4 m). The cylindrical cavity was exposed to the flow environment along its entire length through a slit covered by a resistive screen. The discrimination of such probe systems against flow-generated noise depends upon the interference of pressure disturbances excited inside the tube when phase velocities inside and outside are different. Also, further development of the slit probe concept has been pursued by Noiseux, Noiseux, and Kadman (ref. 5). Their work consisted of adapting the slit probe system to an airfoil shape to further reduce turbulent pressure fluctuations. They also found that inhomogeneities in the resistive screen dramatically reduce the potential discrimination against flow noise. In any case, these systems are too large for the small-scale environment of interest in laminar-to-turbulent transition in boundary-layer flows.

In contrast with flow duct systems, the typical boundary-layer thickness over an aircraft surface in the laminar-to-turbulent transition region may be relatively small (less than 0.1 m), and the acoustic disturbance frequency range, much higher (about 0.5 to 5.0 kHz). Since it is important that intrusive disturbances of the aerodynamic field be minimized, the probe shape should be streamlined and the lateral dimensions should be small relative to the acoustic and hydrodynamic wavelengths. An additional tool for improving the signal-to-noise ratio is a microprocessor-based signal enhancement technique which can be traded off against the more complex probe design concepts of Neise. Specifically, it is anticipated that useful probes for boundary-layer acoustic measurements can be designed on the basis of a small pressure sensor enclosed by a streamlined probe that accommodates a cavity/orifice acoustic system designed to minimize sensitivity changes due to flow. Sensitivity changes due to mean flow are important in this application because the probe may be traversed across an intense mean shear flow to ascertain acoustic excitation level changes in the boundary layer.

Grazing flow across a probe surface may change the acoustic impedance of the coupling system with unavoidable variation in acoustic sensitivity. However, with careful design, these sensitivity variations can be minimized and perhaps even be made insignificant. For localized measurements in an aeroacoustic field, small orifices offer a convenient means to couple the external acoustic field to the probe sensor/cavity system as opposed to the resistive screen arrangement of Neise. The understanding of orifice behavior in the presence of grazing flow has advanced in recent years. In particular, Hersh and Walker (ref. 6); Goldman and Panton (ref. 7); and Kompenhans and Ronneberger (ref. 8) have investigated orifice impedance changes due to grazing flows, and models have been developed that can be used as a basis for minimizing flow effects on probes using orifice-coupling elements.

In addition to pressure-sensing probes, Davis (ref. 9) has investigated analytically the use of a hot film to measure acoustic fields in the presence of mean flow. The hot film has the outstanding advantage of small size (about 1/100 the size of the pressure sensor) and therefore of being much less intrusive than a microphone probe in a boundary-layer flow environment. The hot film responds intrinsically to the heat transfer rate from its surface, and thus in addition to mass flux, which typically dominates its response, it has the disadvantage of potentially responding to fluctuations in temperature and pressure. Therefore, the hot film can respond to all the acoustic field variables as well as nonacoustic mean flow fluctuating quantities. However, the hot film has been developed into a highly reliable sensor and, because of its unobtrusive character, should be considered as a viable alternative to a pressure-sensing probe in the regions of a boundary layer near the surface where measurement-induced flow disturbance is of critical concern.

The main thrust of this experiment was to apply state-of-the-art instrumentation and data processing procedures to extract coherent acoustic signals from subsonic flow up to a speed of Mach 0.5. A specially designed acoustic pressure probe and hot-film probe were installed in a square 5 cm × 5 cm (2 in. × 2 in.) flow duct supporting only progressive, plane wave propagation over the frequency range of 0.5 to 3.0 kHz. The coherent acoustic responses of the sensor configurations were measured, compared, and critically evaluated to determine flow sensitivity effects. In sections that follow, the experimental setup is described, and an analysis is developed to provide a basis for the comparisons of the pressure probe and the hot-film probe.

SYMBOLS

A,B	parameters in King's law
$\bar{A},\bar{B}$	defined in equations 26(b) and 26(c)
c	sound speed in air
c_{ref}	reference sound speed
d	hot-film diameter
E	bridge output voltage
Gr	Grashof number, ratio of buoyancy force to viscous force
H_f	heat transfer per unit time from hot film to air
I	electrical current through hot film
K_f	thermal conductivity of air
Kn	Knudsen number, ratio of molecular mean free path to hot-film diameter, d
L	active length of cylindrical hot film
M	Mach number of local air flow
M_{CL}	Mach number at centerline of duct

N	constant in King's law
Nu	Nusselt number, heat transfer rate per unit area from hot film to air divided by product of K_f and typical temperature gradient
P	instantaneous pressure
Pr	Prandtl number, ratio of kinematic viscosity to thermal diffusivity
P_{ref}	mean reference pressure
P_s	mean static pressure
P_t	mean total pressure
Re	Reynolds number based on hot-film diameter
R_f	hot-film resistance at local air temperature
R_w	hot-film resistance at operating temperature
S	hot-film surface area
SPL	sound pressure level
T_f	mean local air temperature
T_{ref}, T_∞	reference temperatures
T_s	static air temperature
T_t	total air temperature
T_w	hot-film operating temperature
u	mean flow velocity
V_s	velocity in jet potential core
α	hot-film orientation angle with respect to flow direction
γ	ratio of specific heats for air
μ	viscosity of air
μ_∞	reference viscosity for air
ρ	density of air
ρ_{ref}	reference density for air
τ	ratio of local air temperature to hot-film operating temperature

Subscripts:

hf hot film

Kn derivative with respect to Knudsen number

pp pressure probe

m microphone flush mounted in duct wall

A tilde (~) over a symbol denotes a time-fluctuating quantity.

EXPERIMENTAL SETUP

General Description

Dynamic response comparisons of a pressure probe and a hot-film probe in a controlled, aeroacoustic environment were obtained in the flow impedance test laboratory at the Langley Research Center as shown in the schematic diagram of figure 1. Progressive, coherent acoustic waves were caused to propagate along a hard-wall test section equipped with an axial traversing mechanism. A digital stepping motor was connected to a 1.3-cm (0.5-in.) wide axial traverse bar arrangement precision fitted into a 163-cm (64-in.) slot along the length of the square 5 cm × 5 cm (2 in. × 2 in.) test duct section. Care was taken to minimize air leakage between the sliding mechanical contacts by providing pliable sealing strips set into machined grooves in the tube wall and spring loaded against the sides of the traversing bar. Acoustic waves exiting from the test section were absorbed by an anechoic termination section specially designed to be nonreflective both with and without mean flow present in the tube.

Air flow through the tube was provided by the combination of a pressurized plenum upstream of the test section entrance and a vacuum source at the exit of the termination section. An automatic electromechanical control system maintained constant flow through the test section within about 3 percent of a preset Mach number. Static pressure at the control plane (see fig. 1) in the test section was maintained within about 1 percent of a preset value, and the free-stream static temperature of the air flow was maintained within ±1°C of a preset value by means of electric heaters in the air supply line. The sensing point for the heater control feedback loop was a thermocouple located near the plenum exit. From experience, flow stability was optimum when static pressure at the test section was maintained 5 to 10 mm Hg below local barometric pressure and the static temperature was maintained at ambient temperature (1 mm Hg = 133.3 Pa).

Mean Flow Profiles at Test Section

A detailed schematic diagram of the instrumented test section of the flow impedance tube is shown in figure 2. For mean flow velocity profile measurements, two total pressure rakes were fabricated to occupy minimal space in the test section. One rake was mounted on the axial traverse bar and equipped with a stepping motor to control its vertical position (y-axis). The rake probes were positioned 0.61 cm (0.24 in.) apart, and one probe was positioned in the vertical plane 0.635 cm (0.25 in.) off of the centerline (see fig. 1) of the test section. The other rake

was mounted on the side of the test section to scan the total pressure in the horizontal direction (z-axis). To insure an adiabatic thermal condition at the tube wall, a resistance thermometer was embedded in a section of the lower bottom wall. This temperature measurement was compared with the free-stream static temperature as measured by a specially designed thermocouple probe. Appropriate adjustments were then made in the heater control loop to achieve an adiabatic wall condition.

By controlling the relevant parameters discussed above, representative vertical flow profiles as shown in figure 3 were obtained in the test section control plane for nominal centerline Mach numbers of 0.1, 0.3, and 0.5. As is evident from figure 3(a), considerable data scatter and asymmetry were found for the lowest Mach number. The scatter is probably caused by control system variability, and the asymmetry is probably caused by small air leaks and protuberances. For the pressure and hot-film probe comparisons of interest in this investigation, only the profile in the vertical plane at 0.635 cm (0.25 in.) from the centerline is relevant, since all acoustic measurements were taken on this particular profile scan. However, data from the other total pressure tubes were taken and stored for use in later experiments.

Acoustic Input to Test Section

An electromagnetic, 120-W driver was used to supply acoustic energy to the test section. The driver was coupled to the air supply plenum as depicted in the overall schematic diagram of the facility shown in figure 1. The acoustic waves were guided through the plenum chamber by a high-resistance cylindrical core of the same inside diameter as the exiting tube from the plenum to maximize transmitted acoustic energy from the driver and to attenuate valve noise. With this arrangement, discrete frequency sound pressure levels from about 120 dB to about 147 dB could be obtained in the test section over the frequency range of 0.5 to 3.0 kHz. Power to the driver was monitored and found to be invariant with and without flow. Static pressure on the front and back sides of the driver diaphragm was equalized by means of a vent tube to minimize changes in power output or damage to the diaphragm by pressure transients during operation with flow. Acoustic reflections from the termination caused standing-wave ratios not greater than 1.5 dB for the test frequencies of interest.

Surface pressure fluctuations due to test section turbulence were significant, as would be expected. Figure 4 shows typical narrowband (1-Hz) flow noise spectra taken at the flush-mounted microphone located at the control plane in the test section for the three test Mach numbers of 0.1, 0.3, and 0.5. For the Mach number of 0.1, the sound pressure level (SPL) ranges from about 94 dB at low frequencies down to about 86 dB at the higher frequencies. At a Mach number of 0.3, the spectrum shape is similar, but the SPL is 15 to 20 dB higher. At a Mach number of 0.5, the SPL is 26 to 31 dB higher than at $M = 0.1$.

Instrumentation

A schematic diagram of the instrumentation systems used in the experiment is shown in figure 5. The three different transducers were mounted on the axial traverse bar and are depicted at the top of the figure. They consisted of a 0.635-cm (0.25-in.) condenser-type microphone (protective cap removed), flush mounted at the inside surface of the axial traversing bar (flush-mounted microphone); a strain-gage-type pressure sensor enclosed in a specially designed streamlined probe;

and a mass-flux-sensitive hot film, operating in a commercial anemometer bridge circuit with a feedback control loop to provide a constant operating temperature. After signal conditioning appropriate for each transducer system, the output signals were multiplexed through a 50-Hz bandpass tracking filter into a digital signal averager which extracted that part of the fluctuating signal coherent with the acoustic driver input signal. The time-domain-enhanced signal was then analyzed by means of a Fast Fourier Transform computer code implemented with the on-line computer. The fundamental component amplitude of the coherent signal was then processed digitally to produce quantitative comparisons of the acoustic field measurements inferred from the three transducer outputs. Details of the analysis underlying the comparison procedure are described in the "Analysis" section.

A schematic diagram (not to scale) of the pressure probe is shown in figure 6. The cylindrical cavity and orifices that transmit pressure fluctuations to the pressure sensor can be modeled as an acoustic resonator. The cavity resonance was placed at approximately 2.5 kHz, so that over most of the operating frequency range of 0.5 to 3.0 kHz, the response of the resonator was primarily controlled by its stiffness. However, the resonance condition provided a maximum susceptibility to flow-induced sensitivity changes. The ratio of the length to the diameter of the orifice was made as large as was practical (about 1.0) to minimize the effect of the grazing flow on the total orifice impedance. A one-dimensional analysis performed on the probe acoustic system indicated that the pressure drop through the orifice/resonator system would be approximately 3.3 dB for the worst situation, consisting of Mach 0.5 flow and an acoustic signal frequency of 2.5 kHz. Changes in the orifice impedance due to grazing flow were estimated on the basis of a model by Hersh and Walker (ref. 6). The probe design described above was fabricated and equipped with a 0.23-cm (0.09-in.) diameter strain-gage-type pressure sensor installed in a 0.32-cm (0.125-in.) diameter stainless steel tube probe. To minimize the sensor response to static pressure, a vent tube was coupled to the outside of the probe through the orifice as indicated in the diagram of figure 6.

The hot-film probe used in this experiment was of standard design for use in air. The sensor rod (substrate) consisted of high-purity fused quartz with a protective coating of alumina. The sensing film was pure platinum bonded to the quartz rod. The sensing length, L, was 0.508 mm (0.020 in.), and the diameter, d, was 0.025 mm (0.001 in.), with a separation distance between probe supports of 1.27 mm (0.05 in.) to provide a ratio of sensitive length to diameter of 20. The upper limit of the frequency response was 300 kHz.

ANALYSIS

Approach

Since the purpose of this experiment was to compare the coherent acoustic responses of a pressure probe and a hot-film probe in an acoustic wave field convected by a mean flow through a flow duct, the probe responses were correlated with the aid of a third pressure sensor (condenser microphone) flush mounted in the flow duct wall. The flush-mounted microphone and hot-film probe respond predominantly to two different acoustic field quantities, pressure and mass flux, respectively; thus, it was necessary to relate the responses on a common basis by means of the acoustic wave equation. Unfortunately, the hot film is also capable of secondary responses to pressure and temperature fluctuations. Because of this potential response to several acoustic field quantities, it was thought reasonable to adopt a correlating parameter that emphasizes the dominant response mechanism of the hot film, that is,

mass flux. Therefore, it was convenient to correlate the responses in terms of fluctuating acoustic Reynolds number. The procedure was to use acoustic propagation equations with mean flow to infer fluctuating Reynolds number at the hot-film location from acoustic pressure measurements using the flush-mounted microphone. The flush-mounted microphone response was assumed to be unaffected by the grazing flow. For completeness, the hot-film responses were also converted into fluctuating pressure for direct comparison with the responses of the flush-mounted microphone.

Hot-Film Response in Terms of Fluctuating Reynolds Number

Heat removal by forced convection from a cylindrical surface is the basic transduction principle underlying the operation of the hot-film probe. The heat removal rate per unit length, or Nusselt number, is defined as the heat transfer rate to the fluid per unit area, H_f/S, divided by the product of the fluid thermal conductivity, K_f, and a typical temperature gradient. Taking the typical temperature gradient as $(T_w - T_f)/d$, the Nusselt number becomes for a cylinder of diameter d,

$$Nu = \frac{H_f}{\pi L K_f (T_w - T_f)} \tag{1}$$

According to Bradshaw (ref. 10), the power dissipated to the surrounding fluid by an electrically heated hot film can be empirically characterized by a generalized form of the well-known King's law as follows:

$$\frac{H_f}{T_w - T_f} \propto \frac{I^2 R_w}{R_w - R_f} = A(T_f) + B\ Re^{1/N} \tag{2}$$

The symbols R_w and R_f represent the film resistances at operating and fluid mean static temperatures, respectively, and A and B are the usual King's law constants, where A may depend on the fluid temperature, T_f. The film Reynolds number is defined as

$$Re = \frac{\rho u d}{\mu} \tag{3}$$

where d is the film diameter. The film resistance is directly proportional to film temperature; thus, by using Ohm's law, equation (2) may be written

$$E^2 = [A(T_f) + B\ Re^{1/N}] T_w^2 \left(1 - \frac{T_f}{T_w}\right) \tag{4}$$

For constant temperature operation, T_w is constant and may be used as a reference temperature. Rewriting equation (4) with T_w^2 absorbed into the parameters A

and B and defining the ratio $T_f/T_w = \tau$, the voltage drop, E, across the film can be related to the nondimensional variables, τ and Re, as follows:

$$E^2 = [A(\tau) + B\ Re^{1/N}](1 - \tau) \tag{5}$$

It is appropriate at this point to consider any other variables in addition to τ and Re that may affect the hot-film response. To accomplish this, the Nusselt number will be discussed further.

In the most general sense, there are seven dimensionless quantities that can affect the thermal response of a hot film, that is,

$$Nu = f\left(Re,\ \tau,\ Kn,\ Gr,\ Pr,\ \frac{L}{d},\ \alpha\right) \tag{6}$$

Thus, in addition to the Reynolds number, Re, and temperature ratio, τ, the hot-film response can also be influenced by three other fluid variables. As indicated in equation (6), these include the Knudsen number, Kn, the Grashof number, Gr, and the Prandtl number, Pr. Also, there are two configurational parameters involved: the ratio of the sensing length to the diameter of the film, L/d, and the angular orientation with respect to the fluid flow direction, α. According to Davis (ref. 9), effects of fluctuating pressure at constant mass flux density and incident temperature can be described at subsonic speeds by the Knudsen number. The Knudsen number is defined as the ratio of the mean molecular free path to the hot-film diameter and can be shown to be proportional to the ratio of Mach number to Reynolds number. The Grashof number, which accounts for buoyancy effects, can be neglected for mean flow speeds above 0.05 m/s, and the Prandtl number, which accounts for thermal diffusivity, is constant (0.71) for the flow parameter range of interest in this experiment. Only one hot-film geometry ($L/d = 20$) was investigated in this experiment, and the film axis was oriented normal to the flow direction (i.e., $\alpha = \pi/2$ rad). Thus, equation (5) needs to be further amended to include a possible dependence on the Knudsen number, Kn.

The explicit dependence of the film response on Knudsen number is not known; however, the work of Davis (ref. 9) and Davis and Davies (ref. 11) suggests that Knudsen number effects can be estimated by including an implicit dependence of the parameters A and B on Knudsen number, that is,

$$E^2 = [A(Kn,\tau) + B(Kn)\ Re^{1/N}](1 - \tau) \tag{7}$$

According to Bradshaw (ref. 10), empirical evidence suggests that small changes in the fluid temperature cause curves of E^2 versus $Re^{1/N}$ to shift parallel to themselves to a fair approximation. The simplest way to account for this behavior is to assume that

$$A(Kn,\tau) = A(Kn)\ \tau \tag{8}$$

It is further assumed that equation (8) will hold for small temperature fluctuations. No physical argument will be set forth for this "quasi-static" assumption other than the observation that experimental evidence supports a similar type of extension to mass flux intensity fluctuations. However, heat transfer due to unsteady mass flux intensity and unsteady thermal gradients originates with different physical mechanisms. Thus, it is not a priori evident that thermal fluctuations can be modeled along the same lines as mass flux intensity fluctuations. Therefore, in the absence of a rigorous analysis of the dynamics, the effect of fluctuating thermal gradients must be established by experiment. Thus the proposed extension of King's law to include an explicit dependence on temperature ratio, τ, and an implicit dependence on Knudsen number, Kn, becomes

$$E^2 = [A(Kn)\ \tau + B(Kn)\ Re^{1/N}](1 - \tau) \tag{9}$$

For the purposes of this investigation, we seek the linearized relationship between fluctuating Reynolds number, $\tilde{Re}$, Knudsen number, $\tilde{Kn}$, ratio of fluid temperature to hot-film temperature, $\tilde{\tau}$, and bridge output voltage, $\tilde{E}$. Specifically, equation (9) is linearized and solved for the fluctuating Reynolds number, $\tilde{Re}$.

Differentiating equation (9) with respect to Kn gives

$$2EE_{Kn} = \left[A_{Kn}\tau + (B\ Re^{1/N})_{Kn}\right](1 - \tau) \tag{10}$$

Time fluctuations of the hot-film output (i.e., bridge voltage) in response to time fluctuations of Kn, τ, and Re are related by

$$2E\tilde{E} = \left[A_{Kn}\tau + (B\ Re^{1/N})_{Kn}\right](1 - \tau)\ \tilde{Kn} + \left[\frac{B}{N}\ Re^{(1-N)/N}\right](1 - \tau)\ \tilde{Re} + A(1 - \tau)\tilde{\tau} - \left[A\tau + B\ Re^{1/N}\right]\tilde{\tau} \tag{11}$$

Combining equations (10) and (11) gives

$$2E\tilde{E} = 2EE_{Kn}\ \tilde{Kn} + \frac{B}{N}\ Re^{(1-N)/N}(1 - \tau)\ \tilde{Re} + A(1 - \tau)\tilde{\tau} - \frac{E^2}{1 - \tau}\ \tilde{\tau} \tag{12}$$

Before proceeding to solve this equation for fluctuating Reynolds number in terms of the remaining fluctuating quantities, it is of interest to discuss the physics underlying the contributions of the various terms to the total fluctuating bridge voltage. For this purpose it is convenient to restate the equation in the form

$$\tilde{E} = \frac{B}{2EN}(1 - \tau)\ Re^{(1-N)/N}\ \tilde{Re} + E_{Kn}\ \tilde{Kn} - \frac{1}{2E}\left[\frac{E^2}{1 - \tau} - A(1 - \tau)\right]\tilde{\tau} \tag{13}$$

As yet, the relative magnitudes of the terms on the right-hand side of equation (13) are not known. It is anticipated that the dominant contribution will be associated with the first term involving fluctuating Reynolds number or mass flux. The second term is the heat transfer from the film to the fluid associated with fluctuating pressure and expressed in terms of fluctuating Knudsen number. Heat transfer is expected to increase with increasing pressure and for a progressive acoustic wave should be in phase with the mass flux term. The third term specifies the contribution associated with temperature fluctuations. The bracketed part of the term is always positive for reasonable temperature ratios and nonzero mean flow (i.e., if $E^2 > A$ and $\tau < 1$). The negative sign for this term indicates that the fluctuating temperature contribution is out of phase with the mass flux term. This result is physically realistic because an increase in fluid temperature causes less heat transfer from the hot film.

Contributions to fluctuating Reynolds number from fluctuating Knudsen number and temperature ratio due to acoustic wave interaction with the hot film were estimated from measurements of acoustic pressure at a flush-mounted pressure sensor in the same plane as the hot film. This necessitated that $\tilde{Kn}$ and $\tilde{\tau}$ be expressed in terms of fluctuating pressure, $\tilde{P}$.

The Reynolds number of the flow about the hot film based on the film diameter, d, is given by equation (3), which can be linearized to give

$$\frac{\tilde{Re}}{Re} = \frac{\tilde{u}}{u} + \frac{\tilde{\rho}}{\rho} - \frac{\tilde{\mu}}{\mu} \tag{14a}$$

Alternatively, by defining fluctuating Mach number as

$$\tilde{M} = \frac{\tilde{u}}{c}$$

equation 14(a) can be written as

$$\frac{\tilde{Re}}{Re} = \frac{\tilde{M}}{M} + \frac{\tilde{\rho}}{\rho} - \frac{\tilde{\mu}}{\mu} \tag{14b}$$

From reference 11, the relation between Knudsen number, Mach number, and Reynolds number is given as

$$Kn = \sqrt{\frac{\gamma\pi}{2}}\,\frac{M}{Re} \tag{15}$$

Linearizing produces

$$\tilde{Kn} = Kn\left(\frac{\tilde{M}}{M} - \frac{\tilde{Re}}{Re}\right) \tag{16}$$

By substitution from equation (14b), equation (16) becomes

$$\tilde{Kn} = Kn\left(\frac{\tilde{\mu}}{\mu} - \frac{\tilde{\rho}}{\rho}\right) \tag{17}$$

This equation, together with the acoustic field equations which follow, is used to express fluctuating Knudsen number in terms of fluctuating pressure.

From reference 12, fluctuating velocity, density, and temperature are related to fluctuating pressure in a progressive wave as follows:

$$\tilde{u} = \frac{\tilde{p}}{\rho c} \tag{18a}$$

$$\tilde{\rho} = \frac{\tilde{p}}{c^2} \tag{18b}$$

$$\tilde{T}_f = \left(\frac{\gamma - 1}{\gamma}\right)\frac{T_f}{P}\,\tilde{p} \tag{18c}$$

According to Schlichting (ref. 13, p. 329), a power law that closely approximates Sutherland's formula for the viscosity dependence on temperature is given by

$$\mu = \mu_\infty\left(\frac{T_f}{T_\infty}\right)^{3/4} \tag{19}$$

where

$$\mu_\infty = 0.0147 \text{ g/m-sec}$$

and

$$T_\infty = 221.9 \text{ K}$$

Therefore, fluctuating viscosity is related to fluctuating temperature by

$$\tilde{\mu} = \frac{3}{4}\,\mu\left(\frac{\tilde{T}_f}{T_f}\right) \tag{20}$$

Combining equation (18c) with equation (20) yields

$$\tilde{\mu} = \frac{3}{4}\left(\frac{\gamma - 1}{\gamma}\right)\mu\left(\frac{\tilde{P}}{P}\right) \tag{21}$$

Recalling that the temperature ratio is defined as T_f/T_w, we can write the equation for fluctuating temperature ratio as

$$\left(\frac{\tilde{T}_f}{T_w}\right)\left(\frac{T_w}{T_f}\right) = \frac{\tilde{\tau}}{\tau} = \left(\frac{\gamma - 1}{\gamma}\right)\left(\frac{\tilde{P}}{P}\right)$$

or

$$\tilde{\tau} = \tau\left(\frac{\gamma - 1}{\gamma}\right)\left(\frac{\tilde{P}}{P}\right) \tag{22}$$

Equation (17), for the fluctuating Knudsen number, can now be written in terms of fluctuating pressure as

$$\tilde{Kn} = Kn\left[\frac{3}{4}\left(\frac{\gamma - 1}{\gamma}\right) - \frac{P}{\rho c^2}\right]\left(\frac{\tilde{P}}{P}\right) \tag{23}$$

When equation (13) is solved for $\tilde{Re}/Re$, the result from equations (22) and (23) becomes

$$\frac{\tilde{Re}}{Re} = \frac{2EN}{B(1 - \tau)\ Re^{1/N}}\left\{\tilde{E} + E_{Kn}\ Kn\left[\frac{P}{\rho c^2} - \frac{3}{4}\left(\frac{\gamma - 1}{\gamma}\right)\right]\left(\frac{\tilde{P}}{P}\right)\right.$$
$$\left. + \frac{1}{2}\left(\frac{\gamma - 1}{\gamma}\right)\left[\frac{E\tau}{1 - \tau} - \frac{A\tau(1 - \tau)}{E}\right]\left(\frac{\tilde{P}}{P}\right)\right\} \tag{24}$$

The parameters A, B, N, and E_{Kn} of equation (24) are assumed to be evaluated by a calibration procedure that holds the parameters Kn and τ constant over the Reynolds number range of interest. The derivative, E_{Kn}, must be estimated from such parametric calibration data. Available standard calibration equipment for a hot film did not permit the kind of parametric calibration procedure needed to rigorously evaluate E_{Kn}. Also, the available calibration procedure permitted τ to vary by a small amount. The ranges for the pertinent variables during the calibration procedure were as follows:

$$44 < Re < 295 \tag{25a}$$

$$0.0025 < Kn < 0.0026 \tag{25b}$$

$$0.534 < \tau < 0.559 \tag{25c}$$

Since the ranges of variation of Kn and τ are small compared with that of Re, the standard calibration system produced flow conditions that approximated constant Knudsen number and constant temperature ratio over the Reynolds number range of interest. For the particular hot-film diameter (25.4 μm) and aeroacoustic parameter ranges explored in this experiment, it will be shown that Knudsen number effects play an insignificant role; however, according to reference 9 this will not be true for hot wires on the order of 5 μm in diameter. In anticipation that the model developed here will apply to such wires, the contribution of fluctuating Knudsen number is maintained in the development. Therefore, the constants A and B are evaluated using

$$E^2 = \bar{A} + \bar{B}\, Re^{1/N} \tag{26a}$$

and

$$\bar{A} = A\tau(1 - \tau) \tag{26b}$$

$$\bar{B} = B(1 - \tau) \tag{26c}$$

Substituting the above in equation (24) gives

$$\frac{\tilde{Re}}{Re} = \frac{2EN}{\bar{B}\, Re^{1/N}} \left\{ \frac{\tilde{E}}{E} + E_{Kn}\, Kn \left[\frac{P}{\rho c^2} - \frac{3}{4}\left(\frac{\gamma - 1}{\gamma}\right) \right] \left(\frac{\tilde{P}}{P}\right) + \frac{1}{2}\left(\frac{\gamma - 1}{\gamma}\right)\left(\frac{E\tau}{1 - \tau} - \frac{\bar{A}}{E}\right)\left(\frac{\tilde{P}}{P}\right) \right\} \tag{27}$$

The constants $\bar{A}$, $\bar{B}$, and N are obtainable from a least squares fit to the bridge output voltage for a hot film in a steady flow. The temperature ratio, τ, is obtained from the operating overheat ratio.

The evaluation of E_{Kn} poses a special problem. The "standard" hot-film calibration procedure (described later) does not allow the effects of parameters Re, Kn, and τ to be separately evaluated. However, Davis and Davies (ref. 11) have constructed an apparatus that allows the bridge voltage dependence on these parameters to be measured. Although their results were not in a form directly amenable to the evaluation of E_{Kn}, a numerical estimate was deduced from their data which is reproduced in figure 7 of this paper. These data were collected for a hot film of the same general type and construction but of different dimensions from the one used in the present investigation. An estimate of E_{Kn} for the hot film used in this

experiment was obtained by estimating the slopes of the curves representing bridge output voltage versus Knudsen number (see fig. 7) in the vicinity of the operating Knudsen number for this experiment (i.e., 0.0026). It is clear from figure 7 that the role of Knudsen number increases with increasing Reynolds number. Because Reynolds numbers in this experiment range up to 295 (see eq. (25a)), it is not evident that Knudsen number effects can be neglected. In figure 8 are shown estimates of E_{Kn} for values of Kn ranging from 0.001 to 0.009. With the exception of the data points for Kn = 0.001, represented by the circles, all the data cluster generally within the boundaries of the straight solid lines. Also, the two curves that bracket the Kn value of 0.0026 have been highlighted by the shaded symbols. A linear approximation to these data was extrapolated to the Reynolds number range of interest in this experiment. It should be noted that E_{Kn} is always negative. Considering the numerical noise associated with the graphical/numerical procedure used to estimate $\Delta E/\Delta Kn$, the results are surprisingly consistent, with the exception of the outlying data points for Kn = 0.001.

Expressing the hot-film response to the acoustic field in terms of fluctuating Reynolds number is one way to compare the hot-film and flush-mounted microphone. This procedure has the advantage of minimizing the use of the acoustic field equations (and thus of avoiding the introduction of extra terms with their respective measurement errors) in determining the response of the hot film. Also, the fluctuating Reynolds number (or mass flux) and pressure caused by an acoustic disturbance in a boundary-layer flow are of fundamental interest with regard to acoustically induced laminar flow transition. Correlating the response of the hot film on the basis of Reynolds number emphasizes the intrinsic mass-flux-measuring capability of the hot film. An alternate, and more straightforward, comparison scheme makes use of fluctuating pressure directly as the correlating parameter. This procedure can be implemented by converting the fluctuating Reynolds number in equation (27) into the equivalent fluctuating pressure by means of the linearized Reynolds number (eq. (14b)), the plane wave acoustic field relation between fluctuating velocity and pressure given in equation (18a), and the equation for fluctuating viscosity in terms of fluctuating pressure (eq. (21)). The result is

$$\frac{\tilde{P}}{P} = \frac{\dfrac{2EN\tilde{E}}{\bar{B}\,Re^{1/N}}}{\left[\dfrac{P}{\rho c^2} - \dfrac{3}{4}\left(\dfrac{\gamma - 1}{\gamma}\right)\right]\left(1 - \dfrac{2EN}{\bar{B}\,Re^{1/N}}E_{Kn}\,Kn\right) + \dfrac{P}{\rho c^2 M} - \dfrac{EN}{\bar{B}\,Re^{1/N}}\left(\dfrac{\gamma - 1}{\gamma}\right)\left(\dfrac{E\tau}{1 - \tau} - \dfrac{\bar{A}}{E}\right)} \tag{28}$$

This comparison procedure tends to obscure the physics underlying the contributions from the various terms and implies that the hot-film transducer is like a pressure probe, when in reality it measures mass flux, a vector quantity. Nevertheless, in the one-dimensional aeroacoustic field of interest in this evaluation, such a comparison is legitimate and will be presented.

Pressure Probe Response in Terms of Fluctuating Reynolds Number

The flush-mounted microphone response in terms of the fluctuating Reynolds number based on the hot-film diameter will be needed to compare these transducers on a fluctuating Reynolds number basis. To that end, equations (14a), (18a), (18b), and (21) can be combined to give

$$\frac{\tilde{Re}}{Re} = \frac{1}{\rho c^2 M}\left[1 + M - \frac{3}{4}\left(\frac{\gamma - 1}{\gamma}\right)\frac{\rho c^2 M}{P}\right]\tilde{P} \tag{29}$$

where $\tilde{P}$ is the fluctuating acoustic pressure as measured by the flush-mounted microphone.

Calibration of Pressure Probe Against Flush-Mounted Microphone

The 0.635-cm (0.25-in.) condenser microphone was calibrated in the standard manner by use of an electrodynamic calibrator which produced a known SPL (114 dB) at 1.0 kHz. This calibration was assumed to hold for the entire frequency range (0.5 to 3.0 kHz) and was found to be repeatable within ±0.5 dB. The pressure probe was mounted on the traversing bar in the hard-wall test section of the flow impedance tube such that the sensor ports could be positioned at the duct centerline in the same plane as the condenser microphone flush mounted on the traversing bar. A plane wave in the absence of mean flow was propagated down the tube past the measurement plane, and a comparison calibration was performed. Knowing the SPL at the condenser microphone allowed the amplitude calibration factors for the pressure probe at each frequency of interest to be determined. Separate calibration factors at each frequency were required, since the response of the pressure probe was not assumed to be flat over the frequency range of interest. This comparison calibration was repeatable within ±0.75 dB.

Hot-Film Calibration Procedure

The hot film was calibrated in the standard manner by positioning the sensor element in the exit potential core of a convergent nozzle that provided the desired range of Reynolds numbers. The Reynolds number in the potential core of the jet based on the film diameter, d, was derived by using the compressible flow equations taken from reference 14 with appropriate changes in notation. These equations are as follows:

$$V_s^2 = \frac{2\gamma}{\gamma - 1}\left(\frac{P_t}{\rho_t}\right)\left[1 - \left(\frac{P_s}{P_t}\right)^{(\gamma-1)/\gamma}\right] \tag{30a}$$

$$\frac{\rho_s}{\rho_t} = \left(\frac{P_s}{P_t}\right)^{1/\gamma} \tag{30b}$$

$$c_t^2 = \gamma\frac{P_t}{\rho_t} \tag{30c}$$

where the subscript s denotes static conditions in the potential core of the jet, and the subscript t denotes stagnation conditions in the plenum chamber. Combining

these equations gives the expression for mass flux at the hot-film location in the potential core as

$$(\rho_s V_s)^2 = \frac{2}{\gamma - 1} \rho_t^2 c_t^2 \left(\frac{P_s}{P_t}\right)^{2/\gamma} \left[1 - \left(\frac{P_s}{P_t}\right)^{(\gamma-1)/\gamma}\right] \tag{31}$$

It is convenient to define a set of reference quantities as follows:

$$\left.\begin{aligned} \rho_{ref} &= 1.205 \text{ kg/m}^3 \\ c_{ref} &= 343.5 \text{ m/sec} \\ P_{ref} &= 760 \text{ mm Hg} \\ T_{ref} &= 293 \text{ K} \end{aligned}\right\} \tag{32}$$

It follows from the equation of state for perfect gases that

$$\rho_t = \rho_{ref} \frac{P_t}{P_{ref}} \frac{T_{ref}}{T_t} \tag{33}$$

and the sound speed is given by

$$c_t = c_{ref} \sqrt{\frac{T_t}{T_{ref}}} \tag{34}$$

Therefore

$$(\rho_s V_s)^2 = \frac{2}{\gamma - 1} (\rho_{ref} c_{ref})^2 \frac{T_{ref}}{T_t} \left(\frac{P_t}{P_{ref}}\right)^2 \left(\frac{P_s}{P_t}\right)^{2/\gamma} \left[1 - \left(\frac{P_s}{P_t}\right)^{(\gamma-1)/\gamma}\right] \tag{35}$$

From the definition of Reynolds number based on the hot-film diameter, d, and the viscosity dependence on temperature given in equation (19), it follows that the Reynolds number in the potential core of the hot-film calibration jet is

$$Re = \left\{ \frac{2}{\gamma - 1} \frac{T_{ref}}{T_t} \left[1 - \left(\frac{P_s}{P_t} \right)^{(\gamma-1)/\gamma} \right] \right\}^{1/2} \rho_{ref} c_{ref} \frac{P_t}{P_{ref}} \left(\frac{P_s}{P_t} \right)^{1/\gamma} \left(\frac{T_\infty}{T_s} \right)^{0.75} \frac{d}{\mu_\infty} \qquad (36)$$

By varying the flow rate (i.e., total pressure in the calibrator nozzle plenum), the nonlinear relationship (eq. (26a)) between bridge output voltage and hot-film Reynolds number can be established. The least squares fit of this calibration data is used in a computer code for extracting fluctuating acoustic quantities. Each value of total pressure, P_t, and bridge voltage, E, is input to a software routine that calculates a calibration curve of bridge voltage versus Reynolds number. This curve fit was found to be accurate within ±1.0 percent and repeatable within ±2.0 percent for the entire test period. An example of such a data fit is shown in figure 9. The dashed vertical lines represent the three nominal test Reynolds numbers used in this experiment. The Reynolds numbers, based on film diameter, d, correspond to centerline Mach numbers of 0.1, 0.3, and 0.5.

RESULTS AND DISCUSSION

Pressure Probe Acoustic Response on Duct Centerline

Figures 10(a) through 10(c) show comparisons of the pressure probe acoustic responses and those of the flush-mounted microphone for the three test Mach numbers. Each figure shows the fluctuating pressure response of the pressure probe normalized by the static pressure plotted against the fluctuating pressure response of the flush-mounted microphone also normalized by the static pressure. For convenience, this normalized fluctuating pressure is expressed in percent. The key designates the six test frequencies used. At each frequency, the acoustic driver was operated at the maximum "safe" input power. The resulting sound pressure levels ranged from 120 to 147 dB, depending on the test frequency. Generally, the higher levels were obtained at the lower frequencies. The solid line represents a least squares fit through the response data, and the dashed line represents perfect agreement between the two transducer responses. The slope, in degrees, and the intercept of the least squares fit are also given in the key. The expression $20 \log(\tilde{P}_{pp}/\tilde{P}_m)$ in decibels is a measure of the agreement between the least squares fit and the line of perfect agreement. This value is indicated on each plot. When the intercept is zero, the ratio $\tilde{P}_{pp}/\tilde{P}_m$ is constant; otherwise, it becomes greater as the origin is approached. Constant-magnitude systematic errors give rise to a nonzero intercept, and constant-percentage systematic errors cause the slope to deviate from 45°. Clearly, any constant-magnitude error will generate large relative error at sufficiently low response. In all the comparisons that follow, both minimum and maximum deviations of the least squares fit are indicated where applicable.

Within the limits of experimental scatter, the comparisons of figures 10(a) through 10(c) suggest that the pressure probe tracks the responses of the flush-mounted microphone in a linear manner for all three Mach numbers. As the Mach number increases from 0.1 to 0.5, the pressure probe response decreases from approximately 98 percent to 73 percent of the microphone response at the highest excitation levels. In terms of decibels (i.e., $20 \log(\tilde{P}_{pp}/\tilde{P}_m)$), this corresponds to a pressure probe

relative sensitivity decrease ranging from 0.2 to 2.1 dB below that of the microphone response as the flow Mach number increases from 0.1 to 0.5. Although some constant deviation is evident from the nonzero intercepts in figures 10(b) and 10(c), the data trends appear to be dominated by constant-percentage-type deviation. The data trends at each Mach number appear to be independent of frequency and sound pressure level over the test parameter ranges investigated.

There are at least two physical mechanisms that can account for the decreasing response of the pressure probe with increasing mean flow Mach number in this particular experimental setup. The most likely mechanism is flow-induced sensitivity changes of the probe sensing ports relative to the sensitivity of the flush-mounted microphone. The second possible mechanism is sound refraction from the region of the duct center toward the duct walls due to the mean flow shear which, in the case of sound propagation in the direction of flow, would tend to decrease the sound level at the centerline relative to that at the wall.

Since there is no frequency dependence observable in the data of figures 10(a) through 10(c), it appears that the sensitivity changes are most likely attributable to flow-induced impedance changes at the probe sensing ports. It is plausible that if the intrinsic impedance of the probe sensing ports were sufficiently large, then flow-induced changes would amount to negligible changes in the total input impedance as seen by acoustic fluctuations. Although the intrinsic probe sensing-port impedance was made large during the design procedure, compromise was necessary to avoid excessive overall sensitivity loss, since the choice of a small sensor size already implied decreased sensitivity.

For the flush-mounted microphone, not only is the input impedance large, but the arrangement of having the microphone diaphragm coplanar with the duct wall plane (and therefore aligned with the mean flow direction) should reduce the effect of flow on the input impedance. This arrangement, as opposed to the open sensing port of the pressure probe, minimizes the discontinuity presented to the mean flow field and thereby avoids a free shear layer over a cavity. The input impedance of the wall microphone is stiffness controlled. According to the manufacturer, the stiffness corresponds to an equivalent volume of less than 0.0005 cm^3. It is plausible that because this very large acoustic impedance is presented to the aeroacoustic environment by a mechanical diaphragm as opposed to an open cavity, the cavity dynamics due to the mean flow are inhibited relative to the same impedance presented by an open sensing port. The sensing-port impedance of the particular probe design used in this experiment was several orders of magnitude less than that of the microphone. If it is assumed then that the impedance of the flush-mounted microphone was not significantly affected by the flow for reasons indicated above, the constant-percentage-type systematic difference is probably attributable to a decrease in the probe sensitivity. Such a change in sensitivity will increase with Mach number and should be included in a calibration correction if accuracy within 2 dB is to be maintained.

Pressure Probe Acoustic Response off Duct Centerline

Figures 11(a) through 11(c) show comparisons of the pressure probe responses and those of the flush-mounted microphone obtained at four transverse locations of the pressure probe. As indicated on the plot, the SPL was not necessarily the same

for each of the locations. The greatest probe displacement from the centerline location was 2.3 cm (0.9 in.) or within 0.25 cm (0.10 in.) of the wall. Examination of the data reveals very nearly the same behavior of the probe response as was observed for centerline data. These results constitute further evidence that the acoustic wave is essentially plane, and therefore, the refractive effects of the measured profiles shown in figure 3 are negligible.

Hot-Film Probe Acoustic Response on Duct Centerline

Figures 12(a) through 12(c) show fluctuating Reynolds number comparisons between the coherent responses of the hot-film probe on the duct centerline (eq. (27)) and those inferred from the flush-mounted microphone (eq. (29)). For the lowest Mach number, 0.1, the hot-film probe generates a slightly nonlinear response relative to that of the flush-mounted microphone, as indicated by the data trend at low frequencies. A least squares straight-line fit through the data produces the solid line with a slope of 43.3° and an intercept of 0.33. For this straight-line fit to the data, the deviation from the flush-mounted microphone response is about 0.1 dB at the highest excitation level (i.e., lowest frequencies) and about 3.2 dB at the lowest excitation level (highest frequencies). The nonlinear behavior at low flow speeds and low frequencies is consistent with the small-signal assumption underlying the linearization procedure. For the higher intermediate flow Mach numbers of 0.3 and 0.5, the responses are about 4.5 and 5.0 dB greater than those inferred from the microphone. To help understand the source of these consistently higher responses, the relative contributions from the mass flux, Knudsen number, and temperature fluctuations were plotted for all three Mach numbers (fig. 13). Clearly, the Knudsen number contribution is not more than about 3 percent and is consequently negligible in all cases. The mass flux contribution drops from 85 percent at Mach 0.1 to about 62 percent at Mach 0.5, whereas the temperature contribution increases in a corresponding manner from 15 percent to about 38 percent.

In view of these results, the hot-film responses were recalculated to exclude the fluctuating-temperature terms (i.e., the terms containing τ in eq. (27)). The results are shown in figures 14(a) through 14(c). Generally, the agreement of the hot-film responses with the flush-mounted microphone responses is improved at the two higher Mach numbers. The greatest discrepancy occurs now for the Mach number of 0.3, for which the hot-film response exceeds the microphone response by only about 3.5 dB, as compared with 4.5 dB when the temperature term was included. Thus the exclusion of the fluctuating-temperature term largely removes the excess response of the hot film with respect to the microphone when the comparison is done on the basis of fluctuating Reynolds number.

The hot-film probe responses were also compared with the flush-mounted microphone responses in terms of normalized fluctuating pressure. The temperature-related term is included in figures 15(a) through 15(c) and excluded in figures 16(a) through 16(c). The general trends are very similar to those shown in figures 12(a) through 12(c) and 14(a) through 14(c), with maximum deviations of 5.7 dB at Mach 0.3 and 6.0 dB at Mach 0.5 with the temperature term included. Again, exclusion of the fluctuating-temperature terms greatly improves the agreement; the maximum deviation of about 2.9 dB occurs at Mach 0.3.

Linear least squares fits of the responses of the pressure probe and the hot-film probe versus the responses of the flush-mounted microphone have been presented in a simple and straightforward manner. For obvious physical reasons, and for

practical application of pressure probes and hot-film probes as acoustic transducers, the comparison curves should have a zero intercept. A "calibration-type" bias can be used to achieve a zero intercept while maintaining the original slope. With this "calibration-bias" included, the maximum deviations are reduced by about 1.0 dB for both types of response comparisons. Thus, to achieve this level of "accuracy," a dynamic calibration must be conducted.

Error Analysis

Random scatter in the measured electrical signals from the transducers used in this experiment was evaluated and found to be about ±1.2 dB relative to a straight-line, least squares fit. This amount of scatter in the "raw" data is believed to be consistent with the calibration repeatability for the flush-mounted microphone and pressure probe of ±0.5 dB and ±0.75 dB, respectively, plus the day-to-day variability of the test parameters.

In addition to random error, there is clearly much opportunity for systematic-type errors to manifest themselves in an experiment of this kind, as is evident from equations (27) and (28), which involve 12 and 11 measured parameters, respectively. A further attempt to identify sources of systematic error arising from measured parameters in the experiment was conducted by allowing all variables to take on the limits of their respective estimated maximum measurement errors, which ranged from 1 percent for B in King's law to 5 percent for the acoustic Mach number. A systematic calculation involving all combinations of measurement errors indicated maximum errors in the inferred fluctuating Reynolds number of about 12 to 16 percent. Likewise, when the hot-film response was expressed in terms of fluctuating pressure, maximum error ranged from 16 to 63 percent. These levels of potential systematic errors, although significant, increase consistently with Mach number and, therefore, do not explain the anomalous discrepancies at the intermediate Mach number.

The suppression of the terms involving fluctuating temperature in equations (27) and (28) and subsequent improved agreement suggest that the hot film does not respond to fluid temperature fluctuations in the manner suggested by the static calibration model given by equations (26). As suggested by the discussion following equation (8) in the "Analysis" section, this development need not be a cause for concern, since there is no a priori reason to expect the static temperature calibration to hold for dynamic temperature response. The fact that the static mass flux calibration curve does provide a realistic dynamic mass flux calibration does not imply that the static temperature calibration should do so.

It appears that the King's law modified to include Knudsen number and temperature effects is not needed, at least for a hot film with the same geometric dimensions used in this experiment, to estimate levels of coherent acoustic waves in mean flows of Mach 0.5 or less. These results are encouraging in that the measurement of the acoustic contribution to fluctuating mass flux intensity in boundary layers appears feasible.

CONCLUDING REMARKS

An experiment was conducted to measure the responses of a hot-film probe and a pressure probe to acoustic excitation in steady flow up to a Mach number of 0.5. Each probe response was compared with the response of a microphone flush mounted in

a duct wall to relate fluctuating quantities in the flow to those beneath the boundary layer. Since the acoustic velocity, density, and temperature can all contribute to the hot-film response and can all be expressed in a composite way as fluctuating Reynolds number, it was convenient to compare the hot-film probe and flush-mounted microphone responses on this basis. This was accomplished by means of the convected wave equation with the assumption of plane wave propagation. Also, because of the one-dimensional aeroacoustic environment in this experiment, all three transducers were correlated directly on the basis of fluctuating pressure.

At the maximum difference, the pressure probe response was 2.1 dB less than that of the flush-mounted microphone response when compared on the basis of fluctuating pressure. The deviation increased with increasing Mach number and was believed to be caused by flow-induced impedance changes at the probe sensing ports. This part of the experiment validated the assumptions in the experimental setup.

For the hot-film probe response, the use of King's law, without the present modification to include explicit temperature dependence, gives better agreement with the flush-mounted microphone response than could be obtained by including fluctuating-temperature effects. Also, at least for this particular type of hot film, Knudsen number (i.e., fluctuating-pressure effects) contributed at most 3 percent to the response at the highest Mach number. At the worst agreement, the hot-film response was only 3.5 dB more than that of the flush-mounted microphone when compared in terms of fluctuating Reynolds number and 2.9 dB more when compared on the basis of fluctuating pressure.

Surprisingly, the agreement between hot-film and flush-mounted microphone responses degraded when fluctuating temperature effects were included. The hot-film response was greater than the flush-mounted microphone response by as much as 5.0 dB and 6.0 dB when compared on the basis of fluctuating Reynolds number and fluctuating pressure, respectively. When a "calibration-bias" was included to recompute the results so that the linear least squares fits through the data would have zero intercepts, there resulted a decrease in the maximum deviation of about 1.0 dB for comparisons of both the pressure probe and the hot-film probe responses versus the responses of the flush-mounted microphone.

These results suggest that with careful calibration procedures, hot films can be used to estimate the acoustic contribution to fluctuating mass flux intensity in a boundary layer subjected to acoustic excitation. Thus, hot films should be capable of operation in the proximity of a surface where a larger pressure probe might cause unacceptable disturbance of the flow field. These data also indicate that the pressure probe provides a good method for accurately measuring acoustic pressure fluctuations in a flow field where the disturbance caused by a streamlined probe is acceptable.

NASA Langley Research Center
Hampton, VA 23665-5225
March 24, 1986

REFERENCES

1. Morkovin, M. V.; and Corke, T. C.: Conceptual Experiments in Transition to Turbulence Through Combined Visualization and Hot-Wire Techniques. ARO 17690.1-EG (Contract SFRC No. DAAG 29-81-K-0012), U.S. Army Res. Office, Apr. 31, 1984. (Available from DTIC as AD A142 193.)

2. Maestrello, Lucio; Parikh, Paresh; Bayliss, Alvin; and Turkel, Eli: Active Control of Compressible Flows on a Curved Surface. SAE Tech. Paper Ser. 851856, Oct. 1985.

3. Neise, W.: The Change of Microphone Sensitivity Under Mean Flow Conditions. J. Sound & Vib., vol. 43, no. 1, Nov. 8, 1975, pp. 53-60.

4. Neise, W.: Theoretical and Experimental Investigations of Microphone Probes for Sound Measurements in Turbulent Flow. J. Sound & Vib., vol. 39, no. 3, Apr. 8, 1975, pp. 371-400.

5. Noiseux, D. U.; Noiseux, N. B.; and Kadman, Y.: Development, Fabrication and Calibration of a Porous Surface Microphone in an Aerofoil. NASA CR-132636, [1975].

6. Hersh, A. S.; and Walker, B.: The Acoustic Behavior of Helmholtz Resonators Exposed to High Speed Grazing Flows. AIAA Paper 76-536, July 1976.

7. Goldman, A. L.; and Panton, Ronald L.: Measurements of the Acoustic Impedance of an Orifice Under a Turbulent Boundary Layer. J. Acoust. Soc. America, vol. 60, no. 6, Dec. 1976, pp. 1397-1404.

8. Kompenhans, J.; and Ronneberger, D.: The Acoustic Impedance of Orifices in the Wall of a Flow Duct With a Laminar or Turbulent Flow Boundary Layer. AIAA-80-0990, June 1980.

9. Davis, M. R.: Hot Wire Anemometer Response in a Flow With Acoustic Disturbances. J. Sound & Vib., vol. 56, no. 4, Feb. 22, 1978, pp. 565-570.

10. Bradshaw, P.: An Introduction to Turbulence and Its Measurement. Pergamon Press, Inc., c.1971.

11. Davis, M. R.; and Davies, P. O. A. L.: Factors Influencing the Heat Transfer From Cylindrical Anemometer Probes. Int. J. Heat & Mass Transfer, vol. 15, no. 9, Sept. 1972, pp. 1659-1677.

12. Pierce, Allan D.: Acoustics - An Introduction to Its Physical Principles and Applications. McGraw-Hill, Inc., c.1981.

13. Schlichting, Hermann (J. Kestin, transl.): Boundary-Layer Theory, Seventh ed. McGraw-Hill Book Co., c.1979.

14. Liepmann, H. W.; and Roshko, A.: Elements of Gasdynamics. John Wiley & Sons, Inc., c.1957.

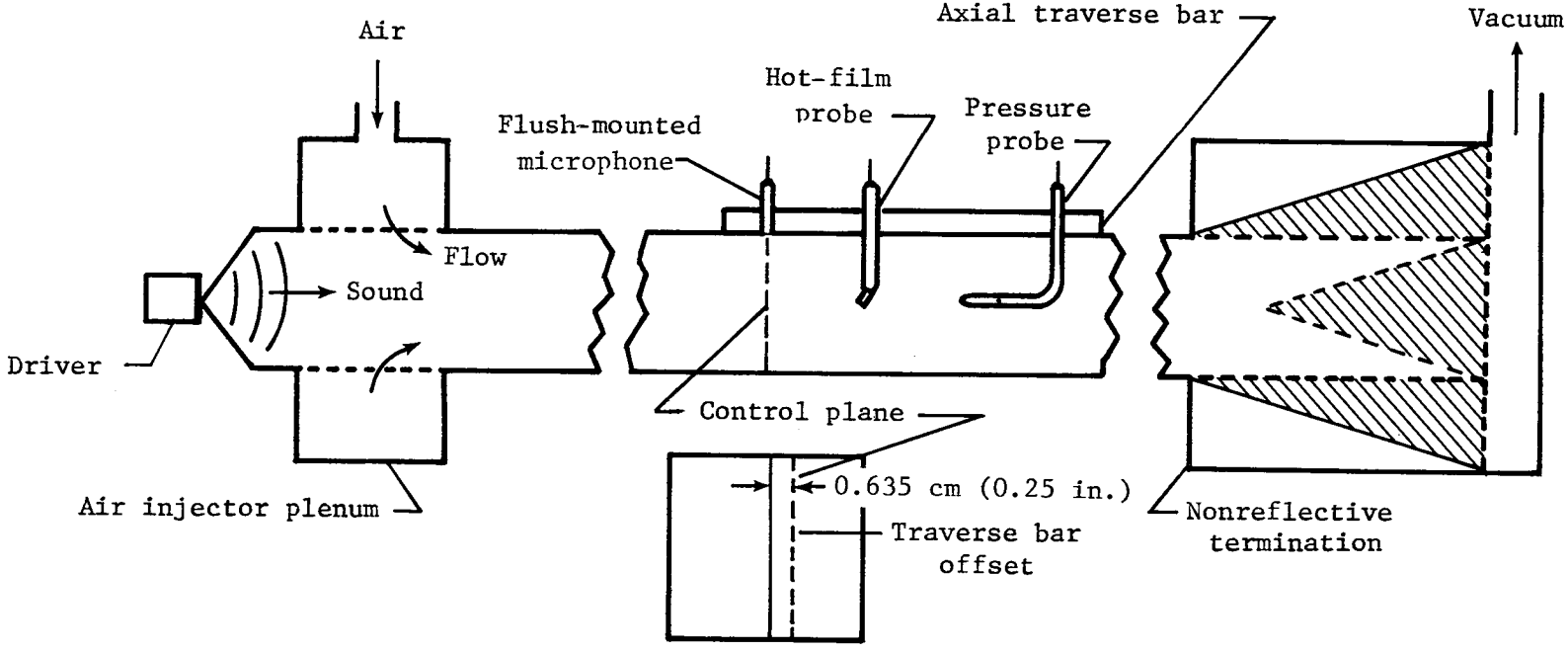

Figure 1.- Schematic diagram of flow impedance tube configured for probe comparison experiment (not to scale).

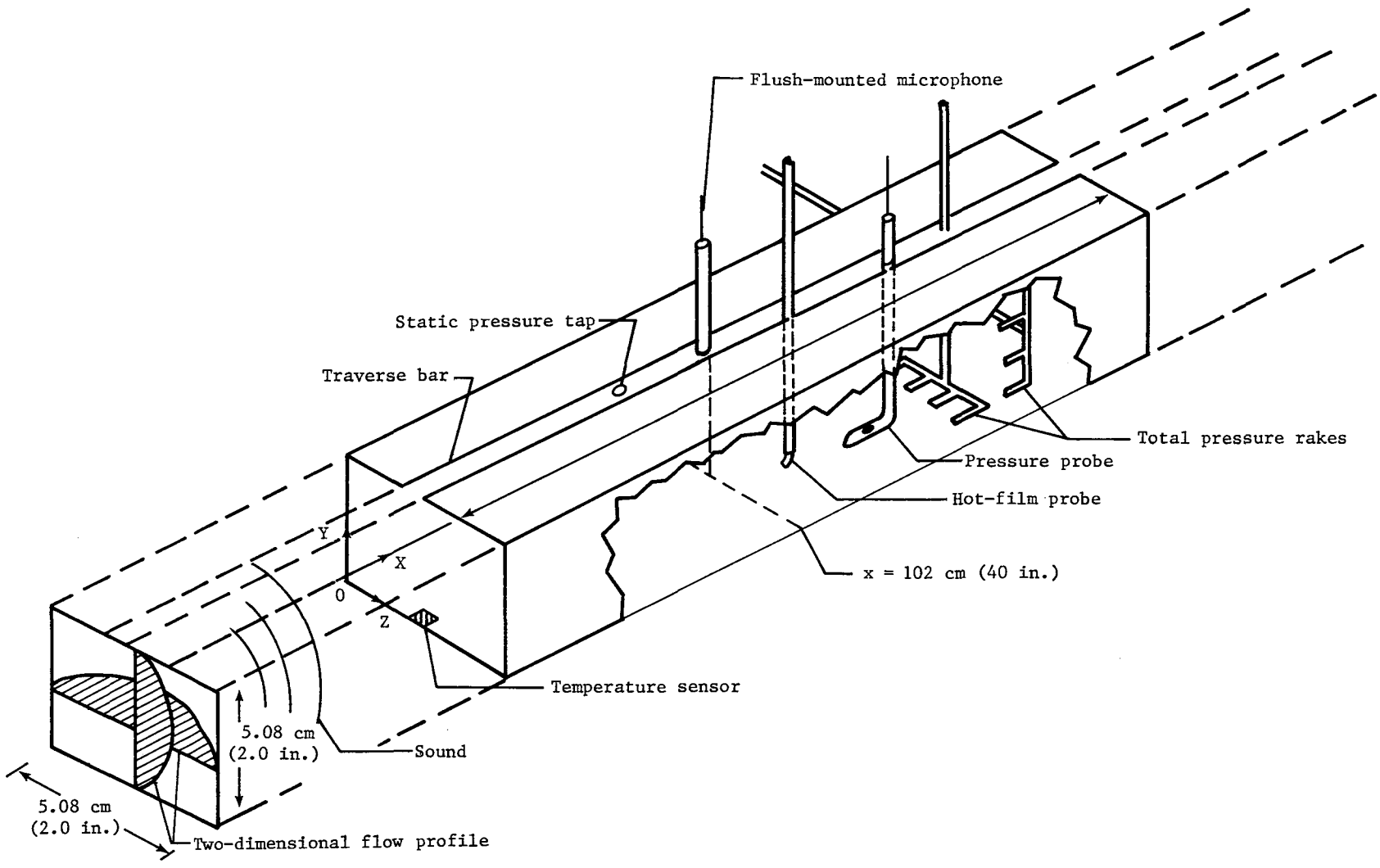

Figure 2.- Schematic diagram of test section and probe arrangement (not to scale).

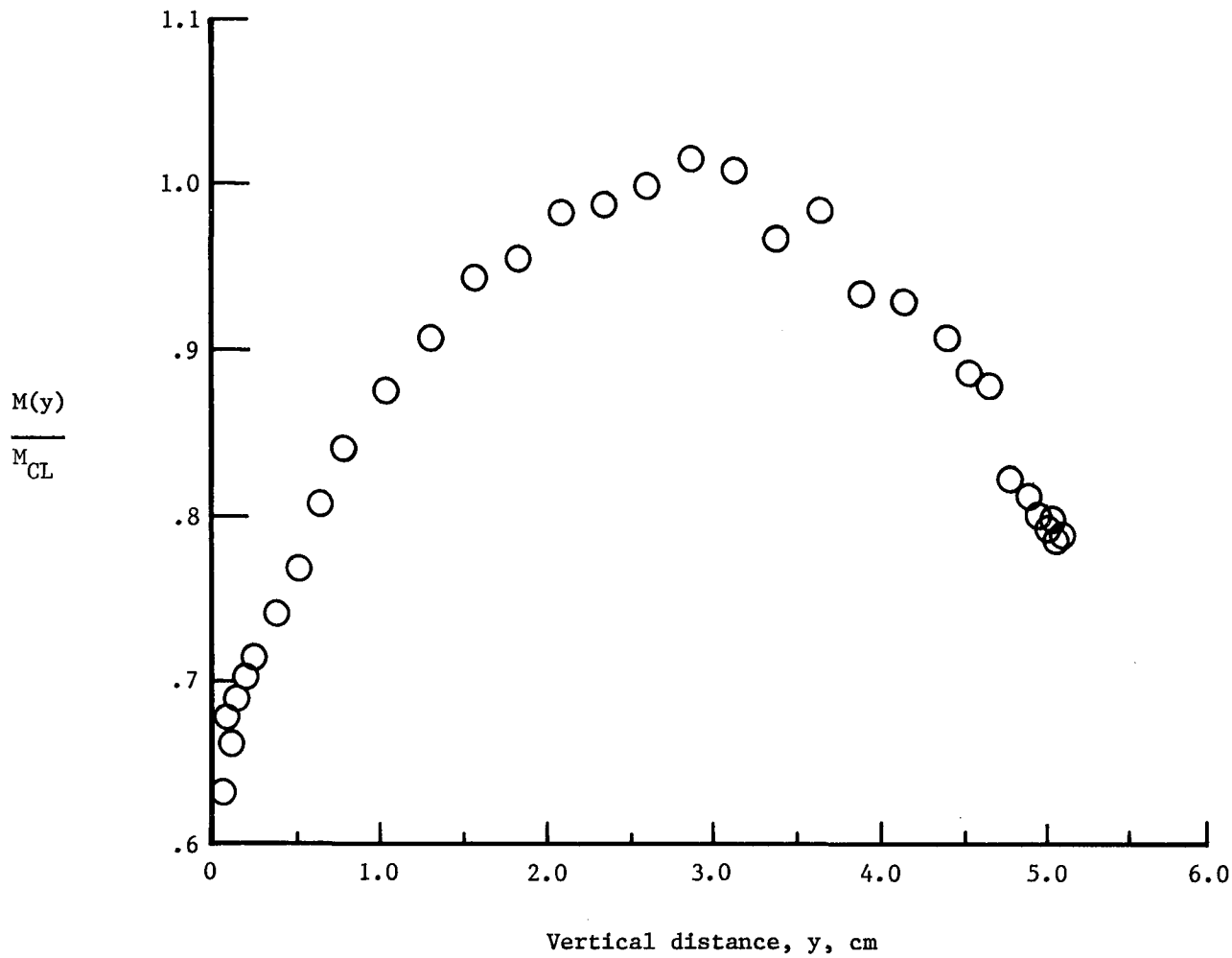

(a) $M_{CL} = 0.1$.

Figure 3.- Measured vertical flow profile at control plane (z = 3.16 cm).

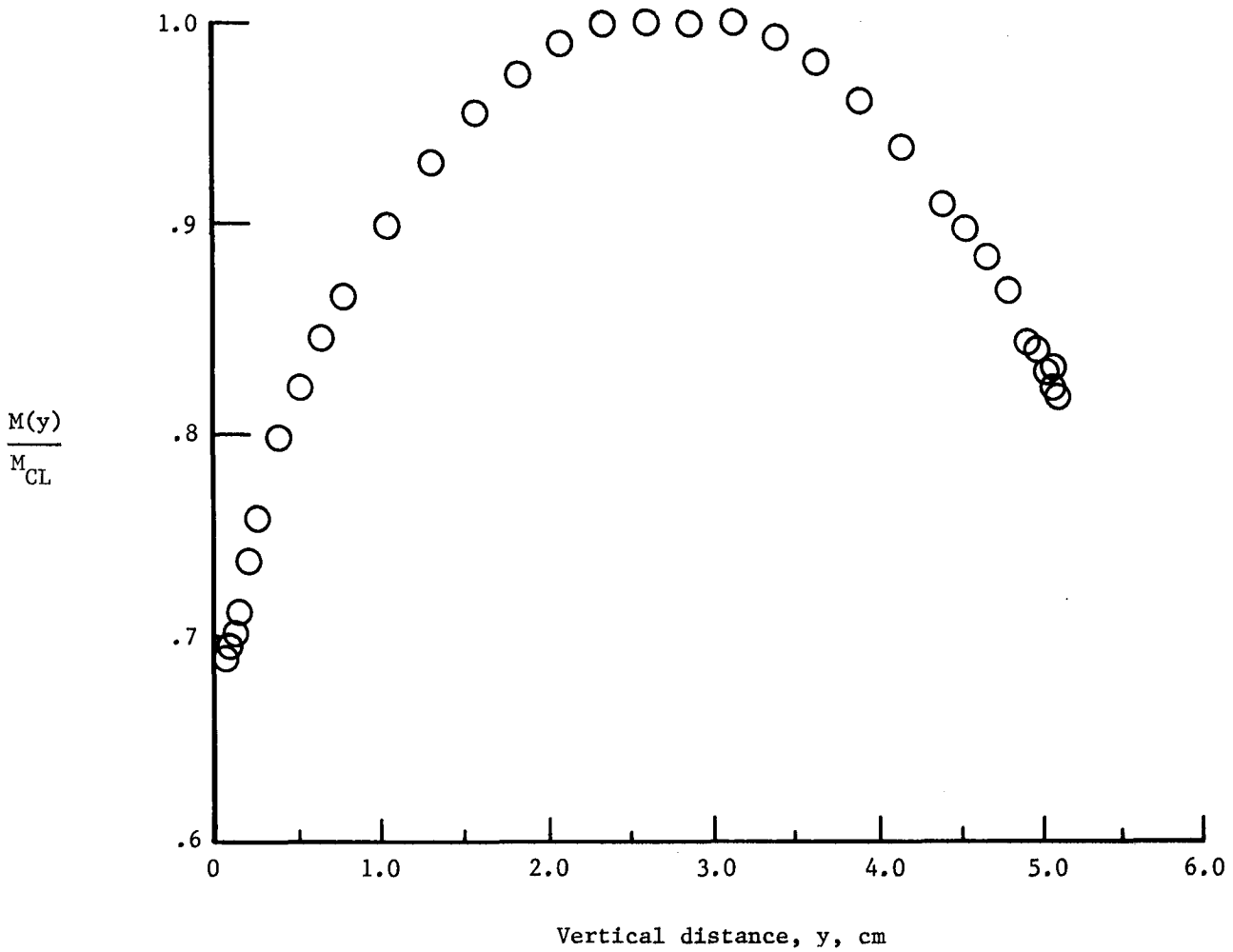

(b) $M_{CL} = 0.3$.

Figure 3.- Continued.

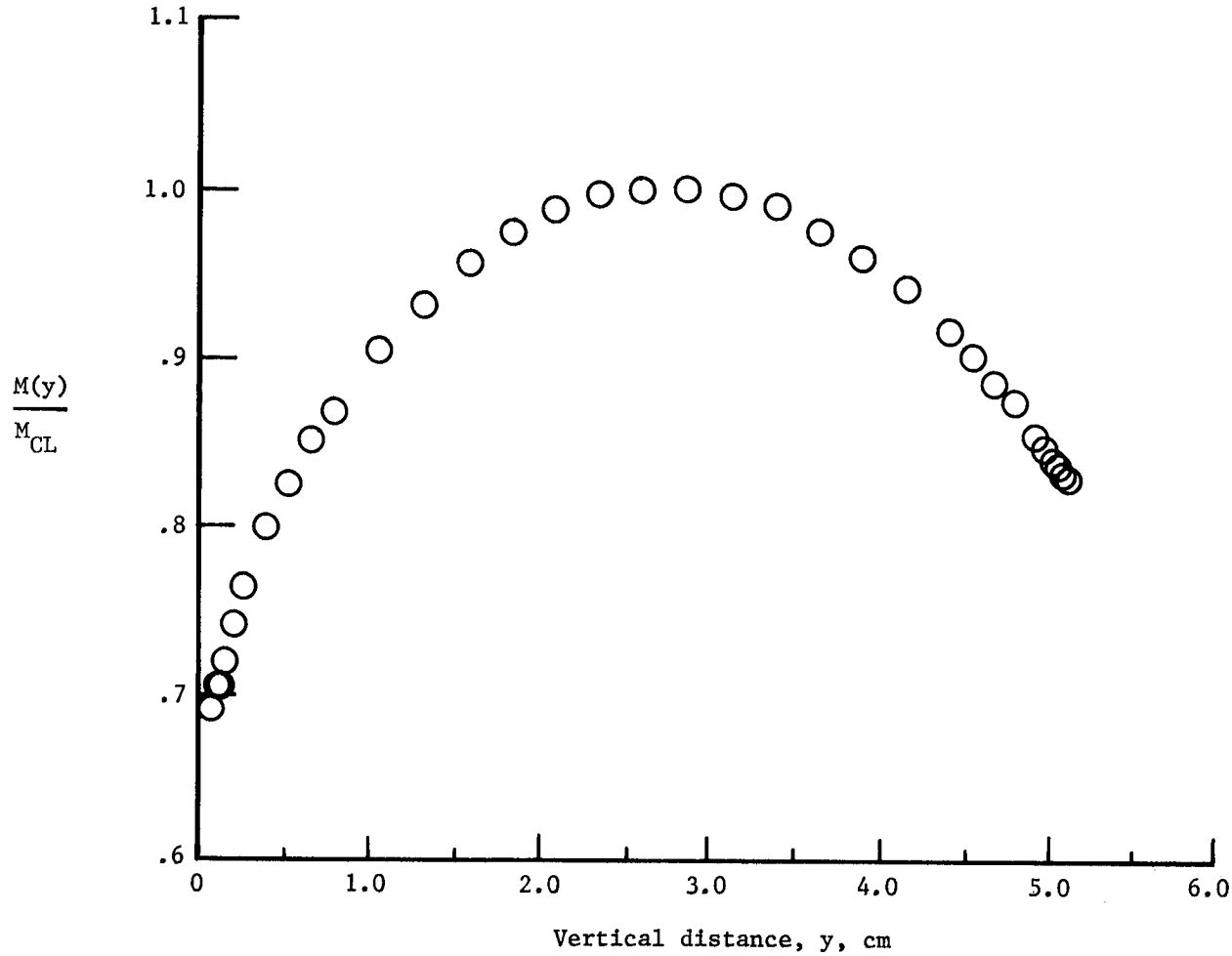

(c) $M_{CL} = 0.5$.

Figure 3.- Concluded.

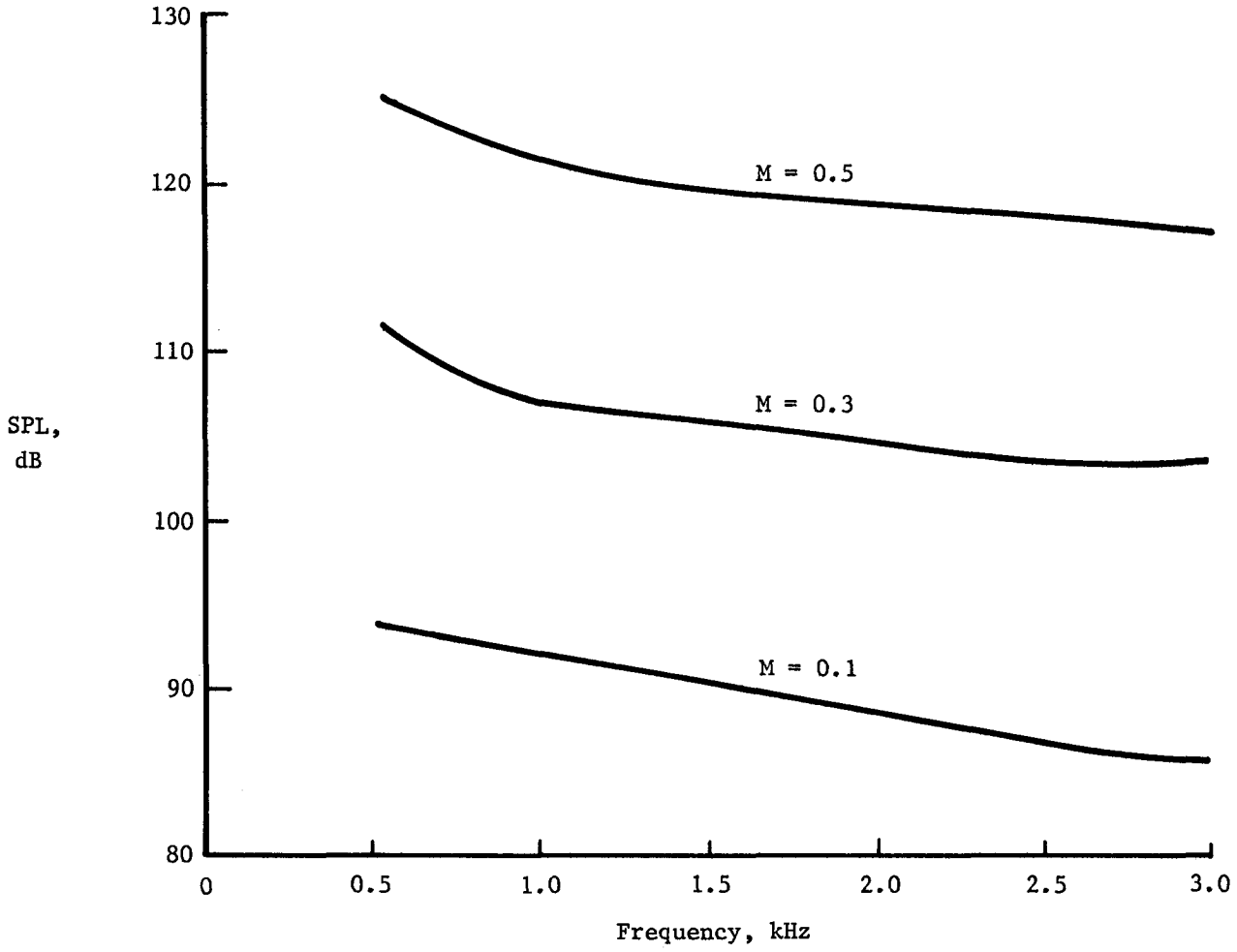

Figure 4.- Narrowband (1-Hz) flow noise spectra.

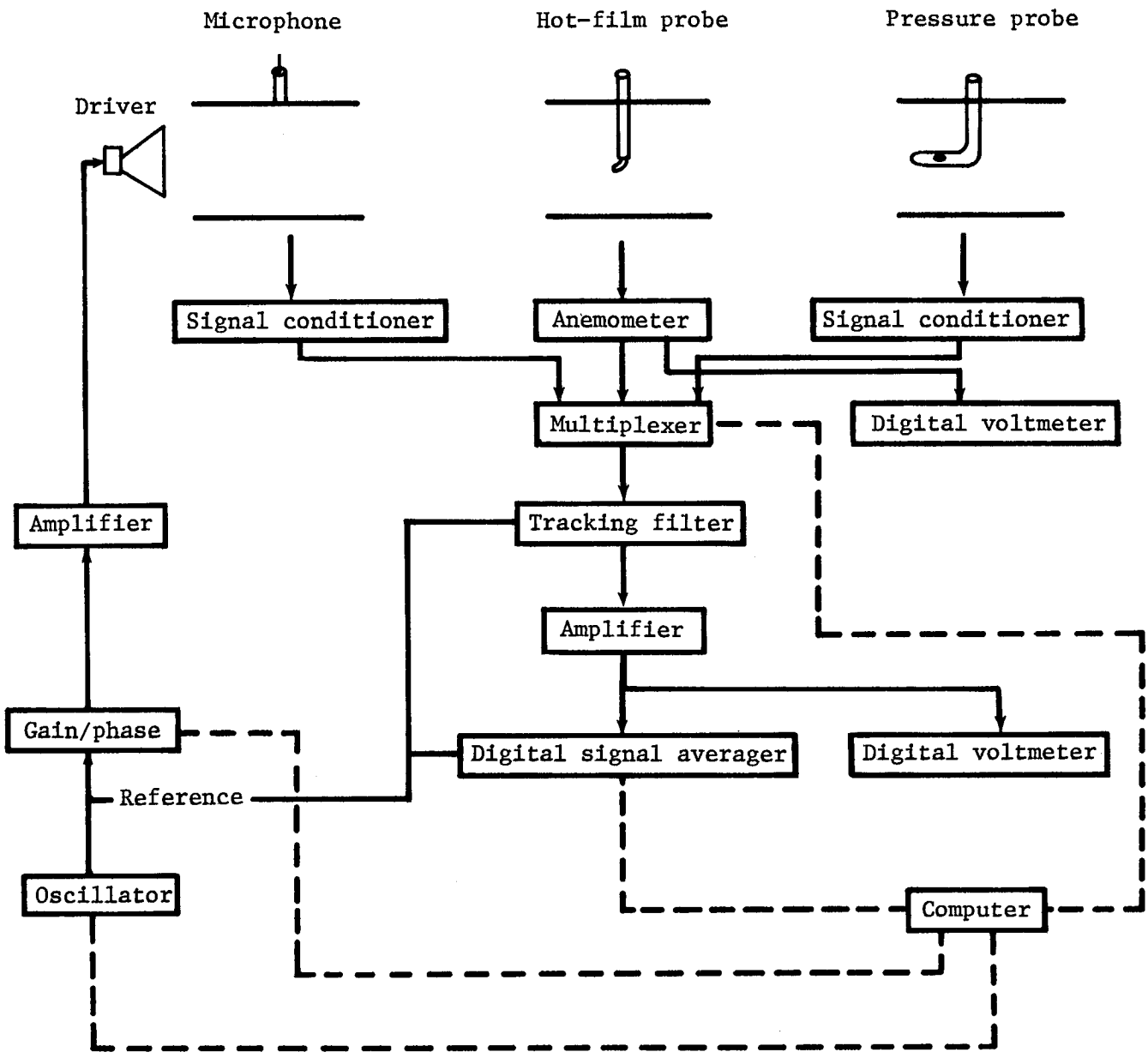

Figure 5.- Schematic diagram of instrumentation.

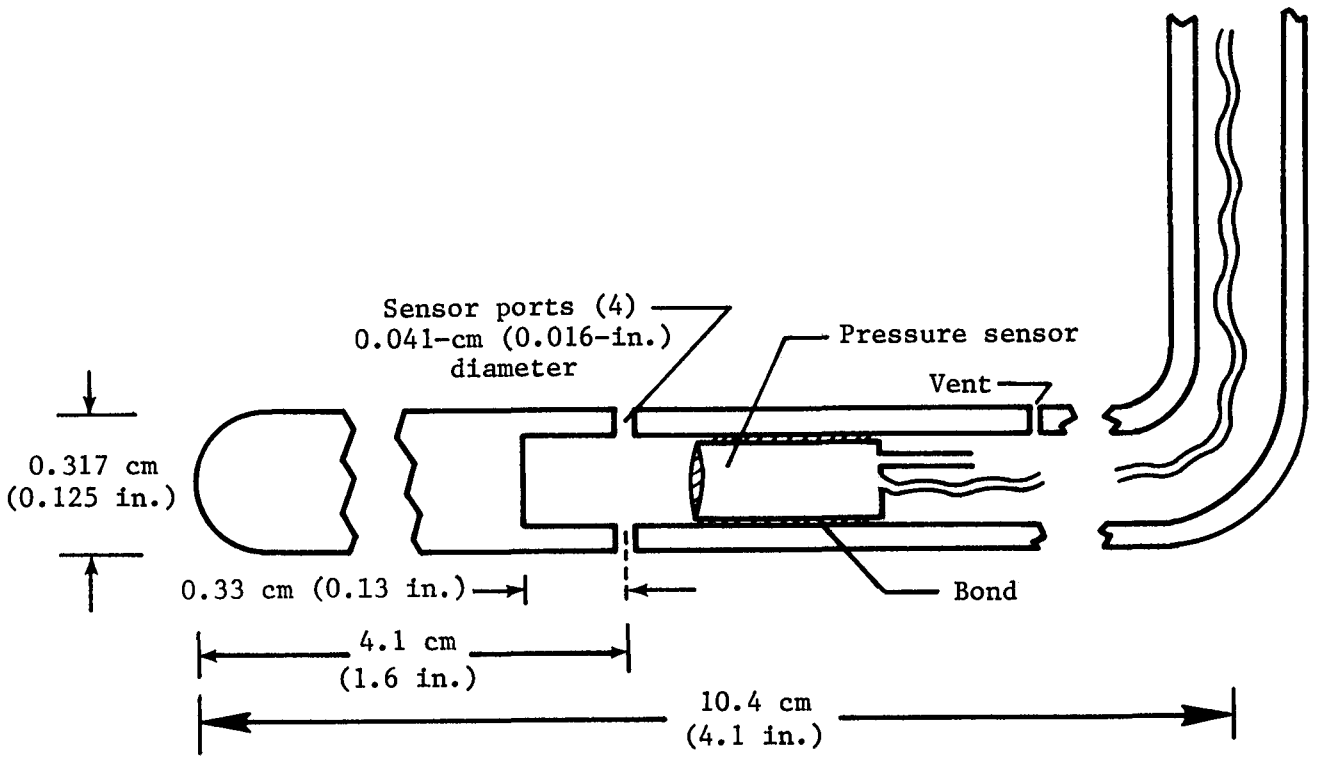

Figure 6.- Schematic diagram of pressure probe (not to scale).

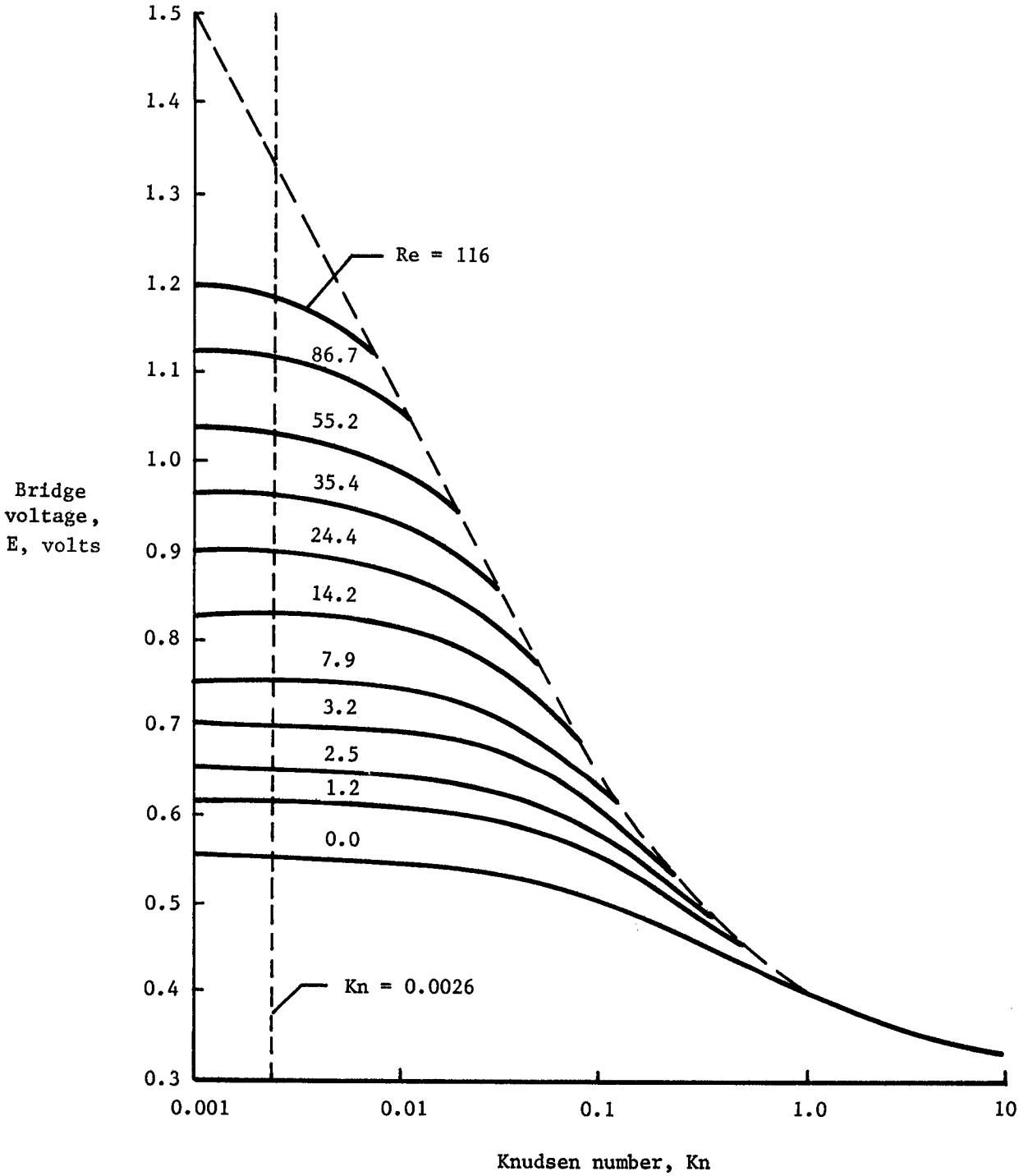

Figure 7.- Bridge output voltage (proportional to heat transfer) from a cylindrical film probe operated in a variable density subsonic stream; Film diameter = 53 μm (from ref. 11).

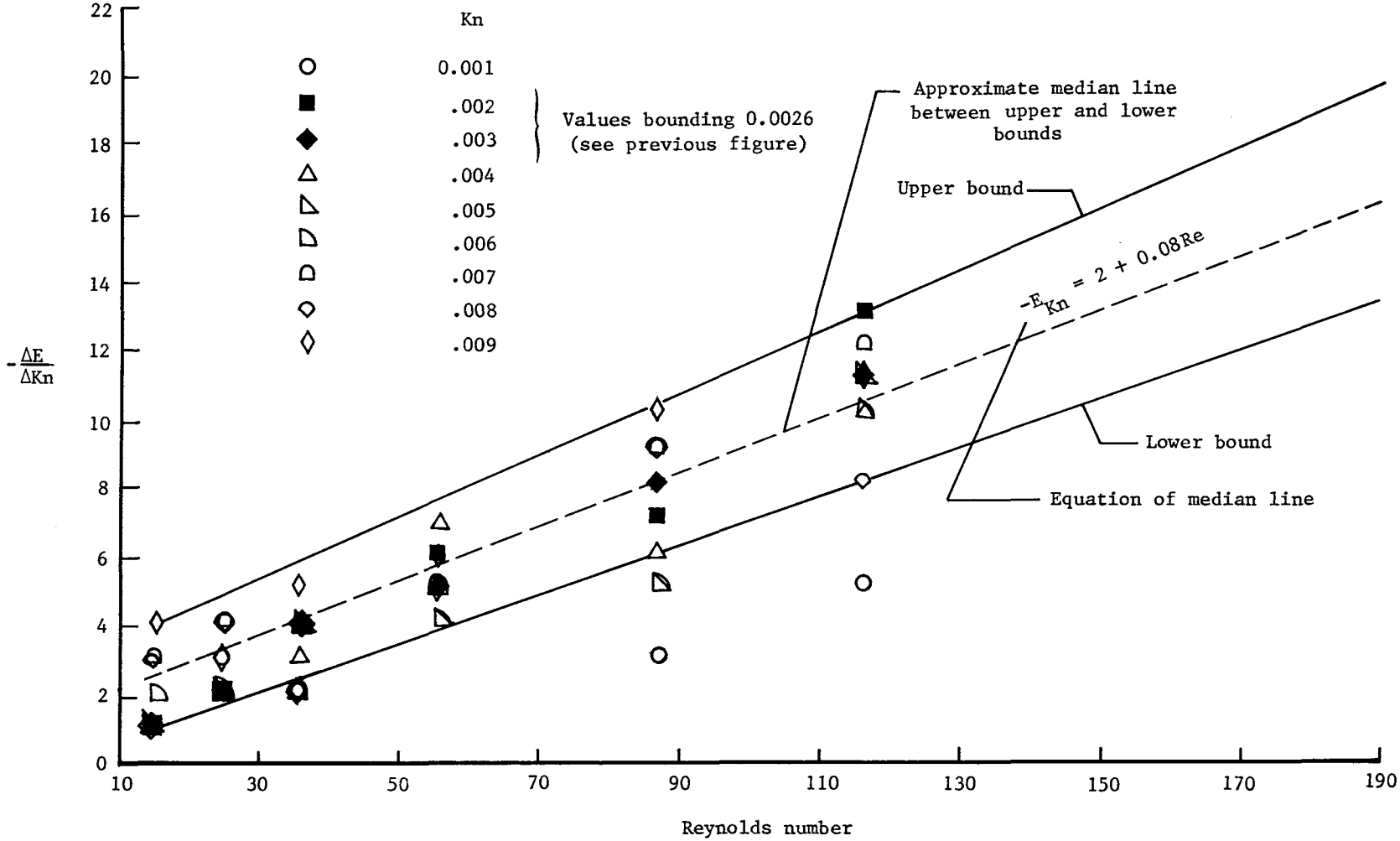

Figure 8.- Numerical evaluation of E_{Kn} from data of figure 7 for a Knudsen number range including 0.0026 for film used in this test.

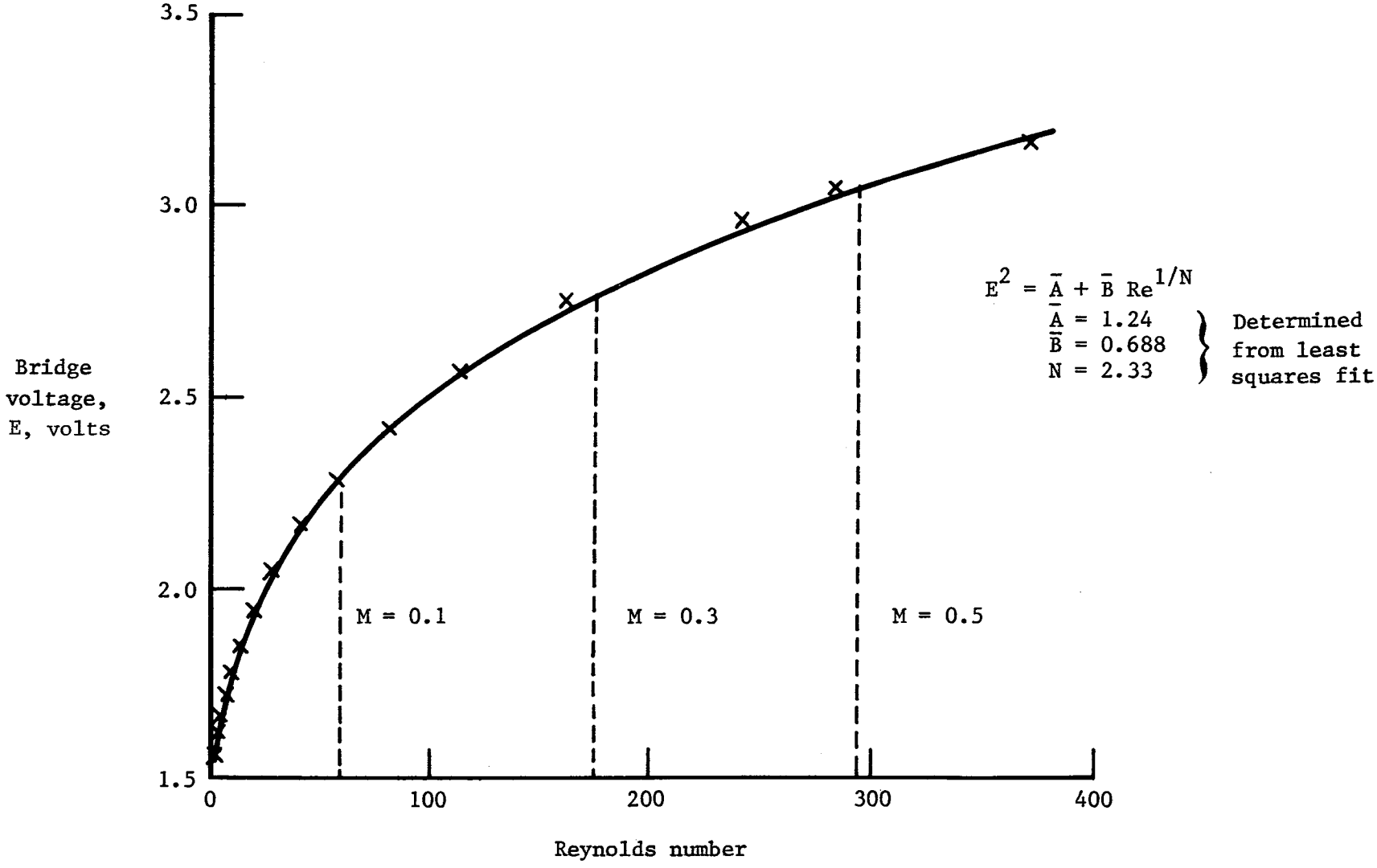

Figure 9.- Typical least squares fit of King's law model to hot-film calibration data.

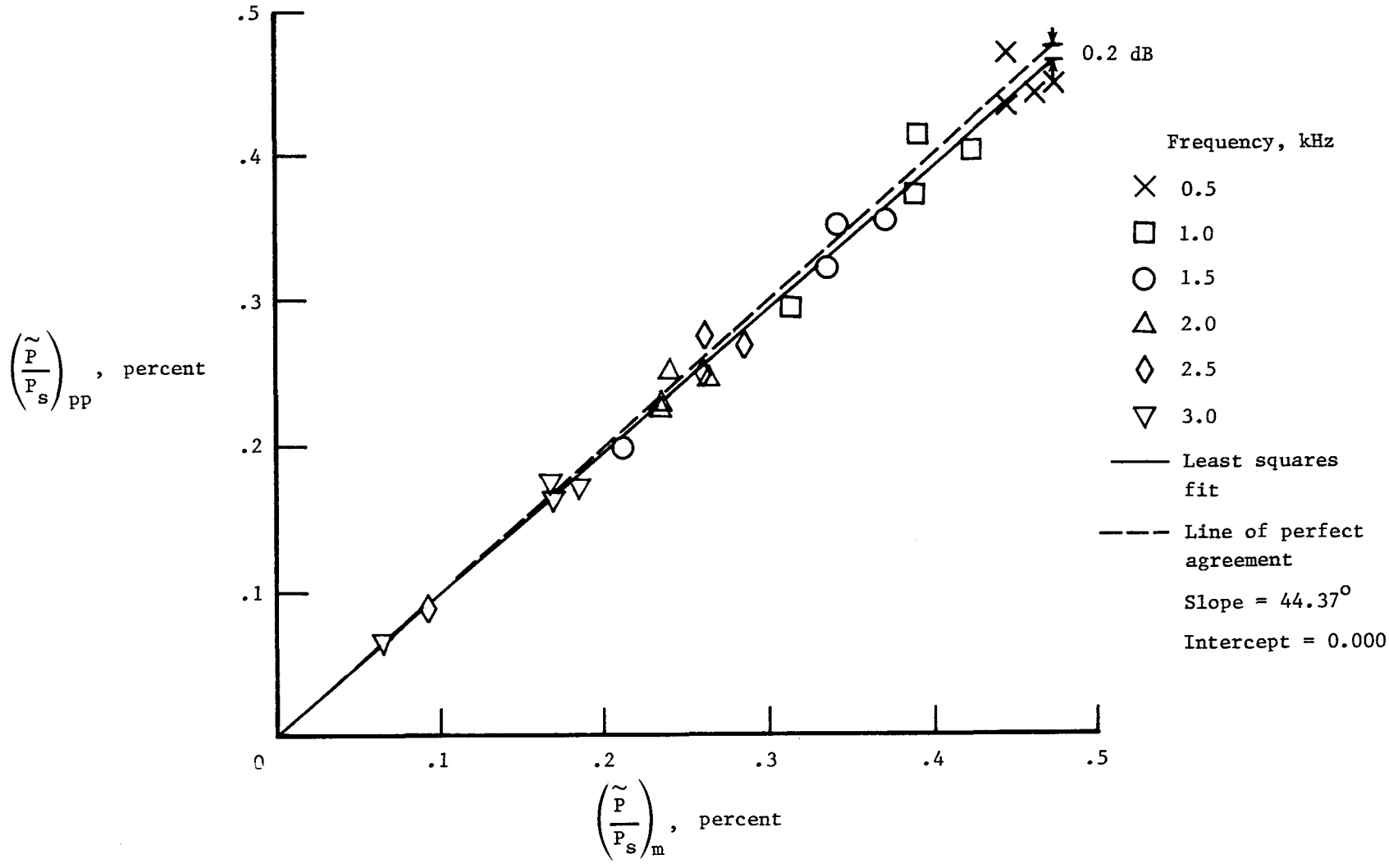

(a) M = 0.1.

Figure 10.- Comparison of pressure probe and flush-mounted microphone responses to acoustic excitation in mean flow.

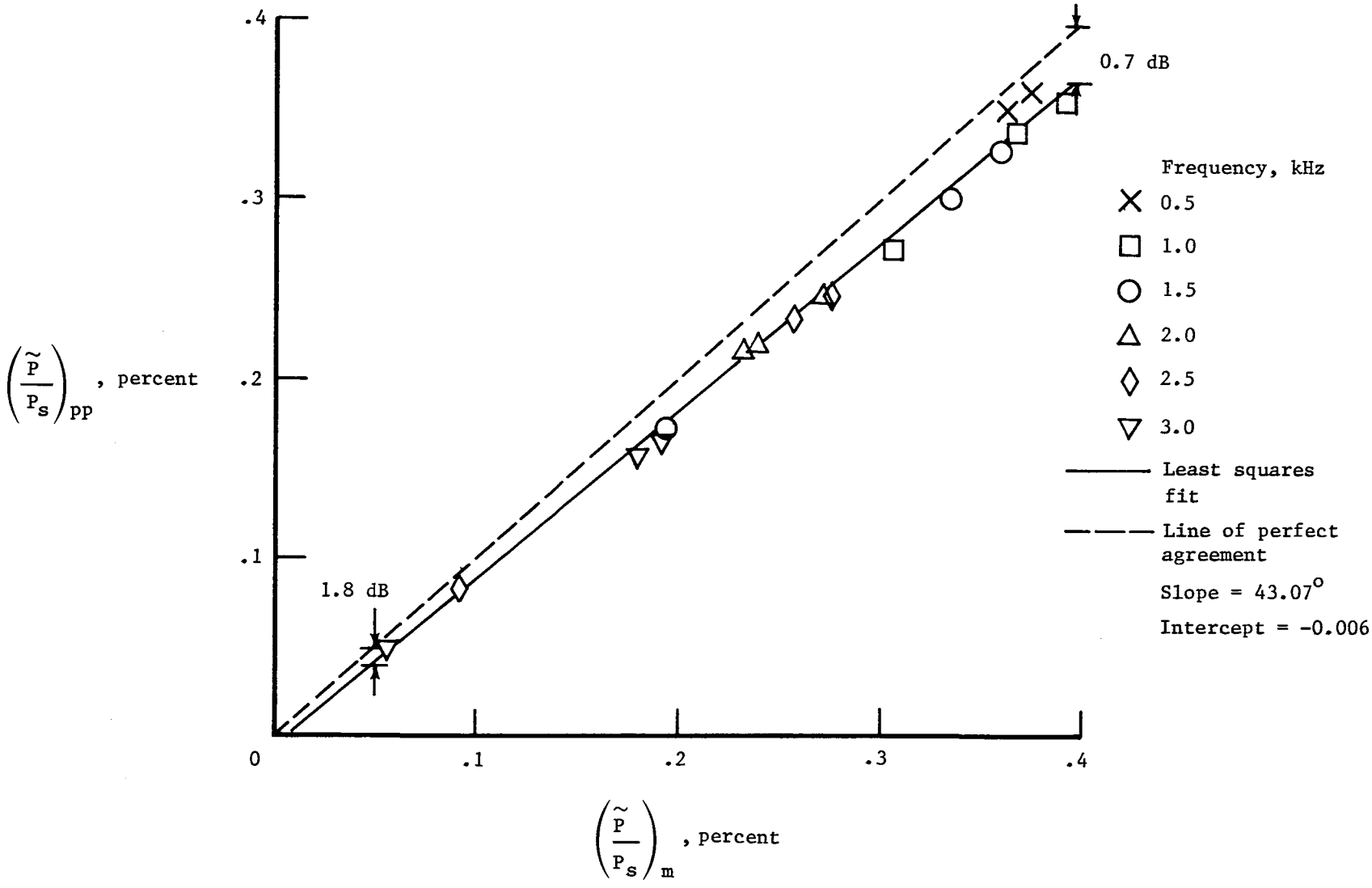

(b) M = 0.3.

Figure 10.- Continued.

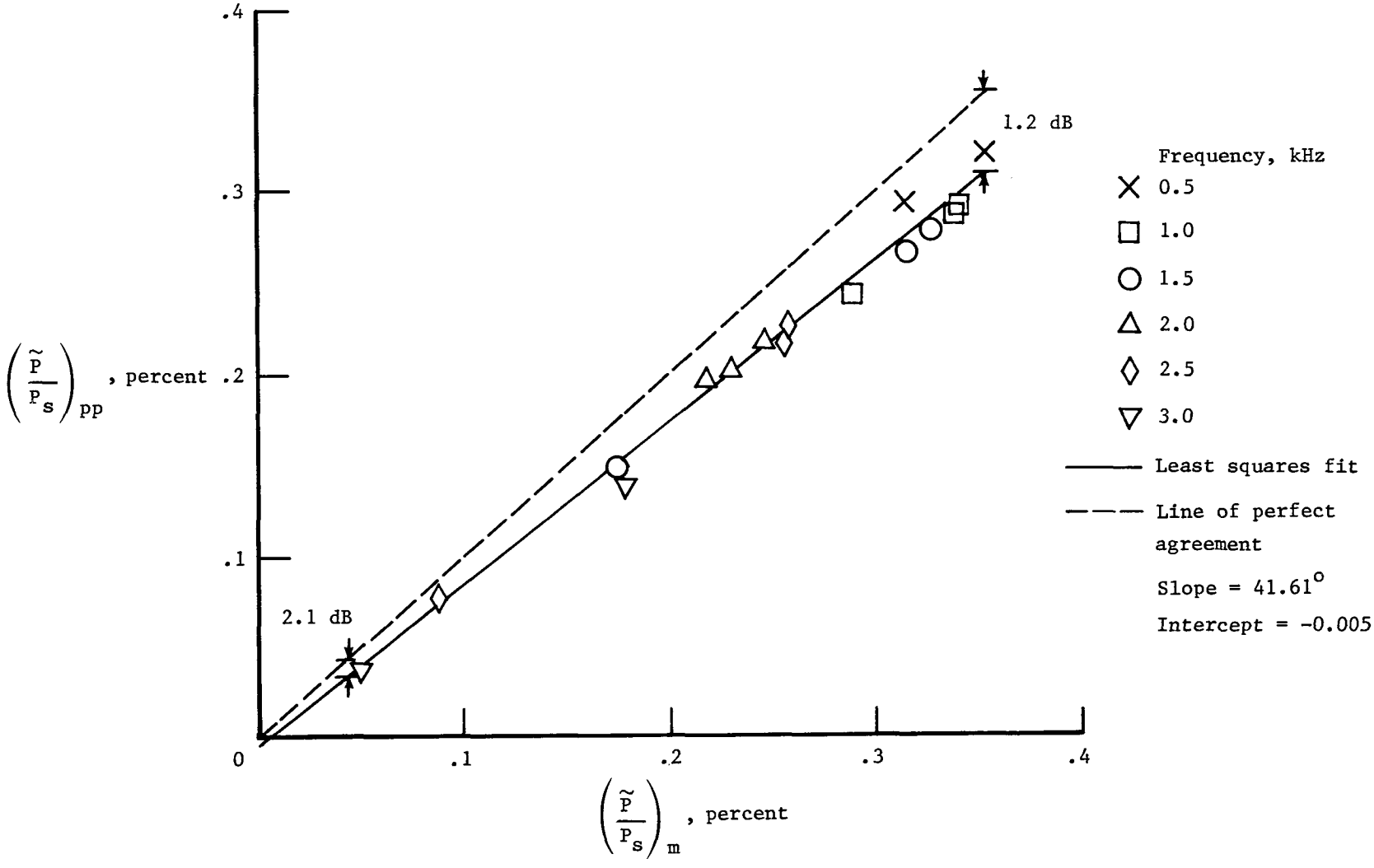

(c) M = 0.5.

Figure 10.- Concluded.

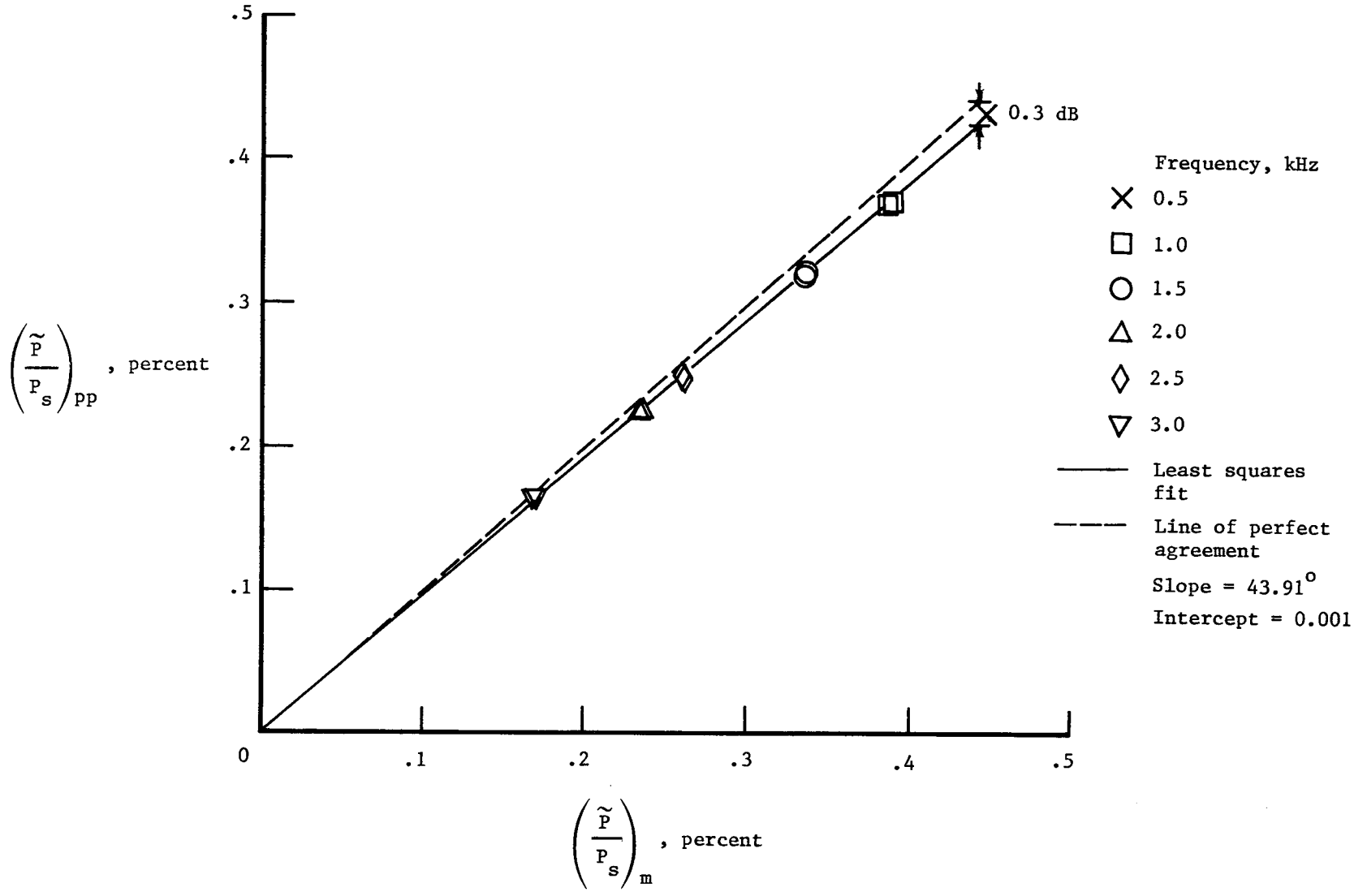

(a) M = 0.1.

Figure 11.- Comparison of pressure probe (four transverse locations) and flush-mounted microphone responses to acoustic excitation in mean flow. Distances from centerline of 0.0, 0.76, 1.5, and 2.3 cm.

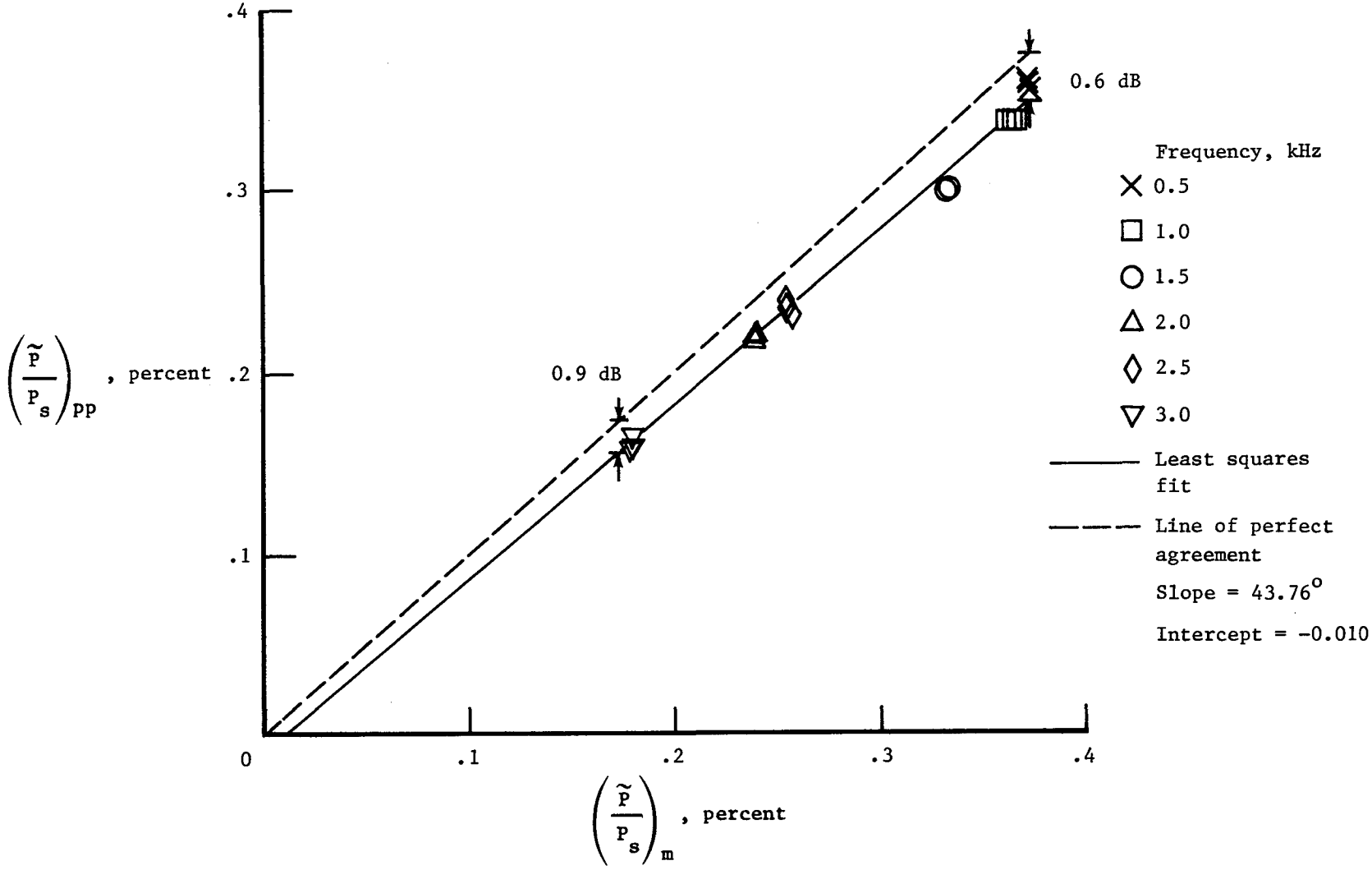

(b) M = 0.3.

Figure 11.- Continued.

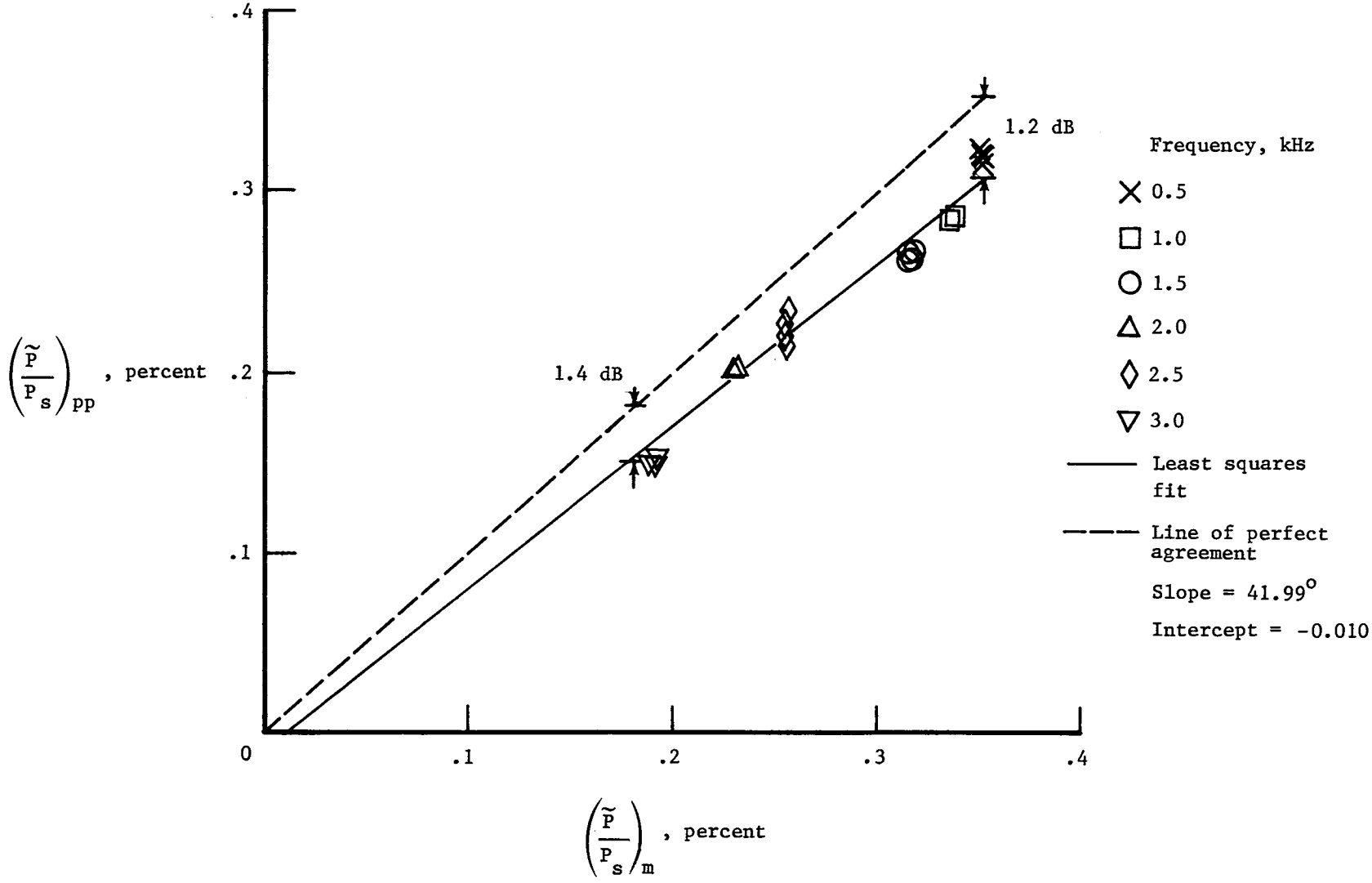

(c) M = 0.5.

Figure 11.- Concluded.

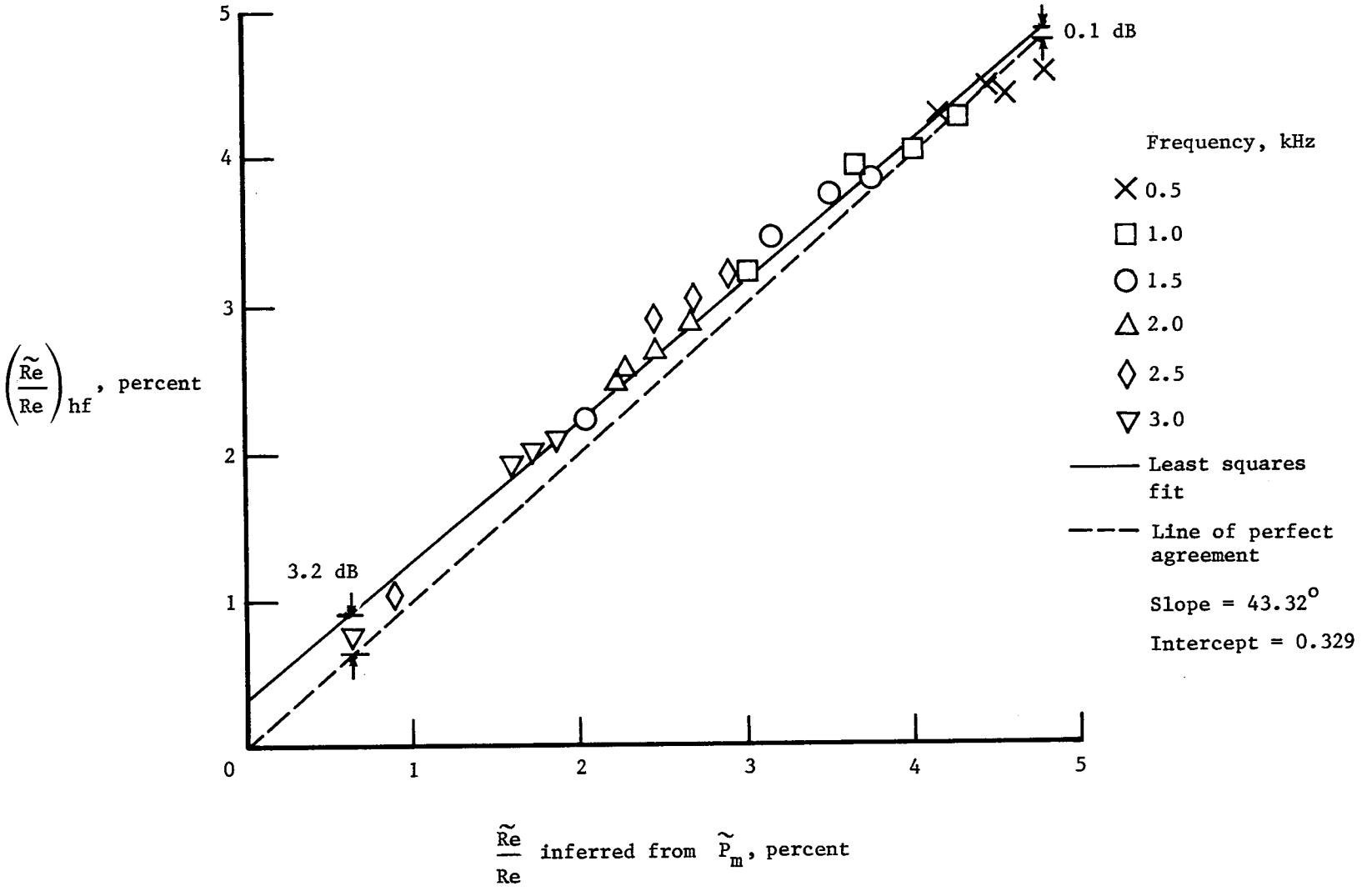

(a) M = 0.1.

Figure 12.- Comparison of hot-film probe and flush-mounted microphone responses (in terms of fluctuating Reynolds number) to acoustic excitation in mean flow.

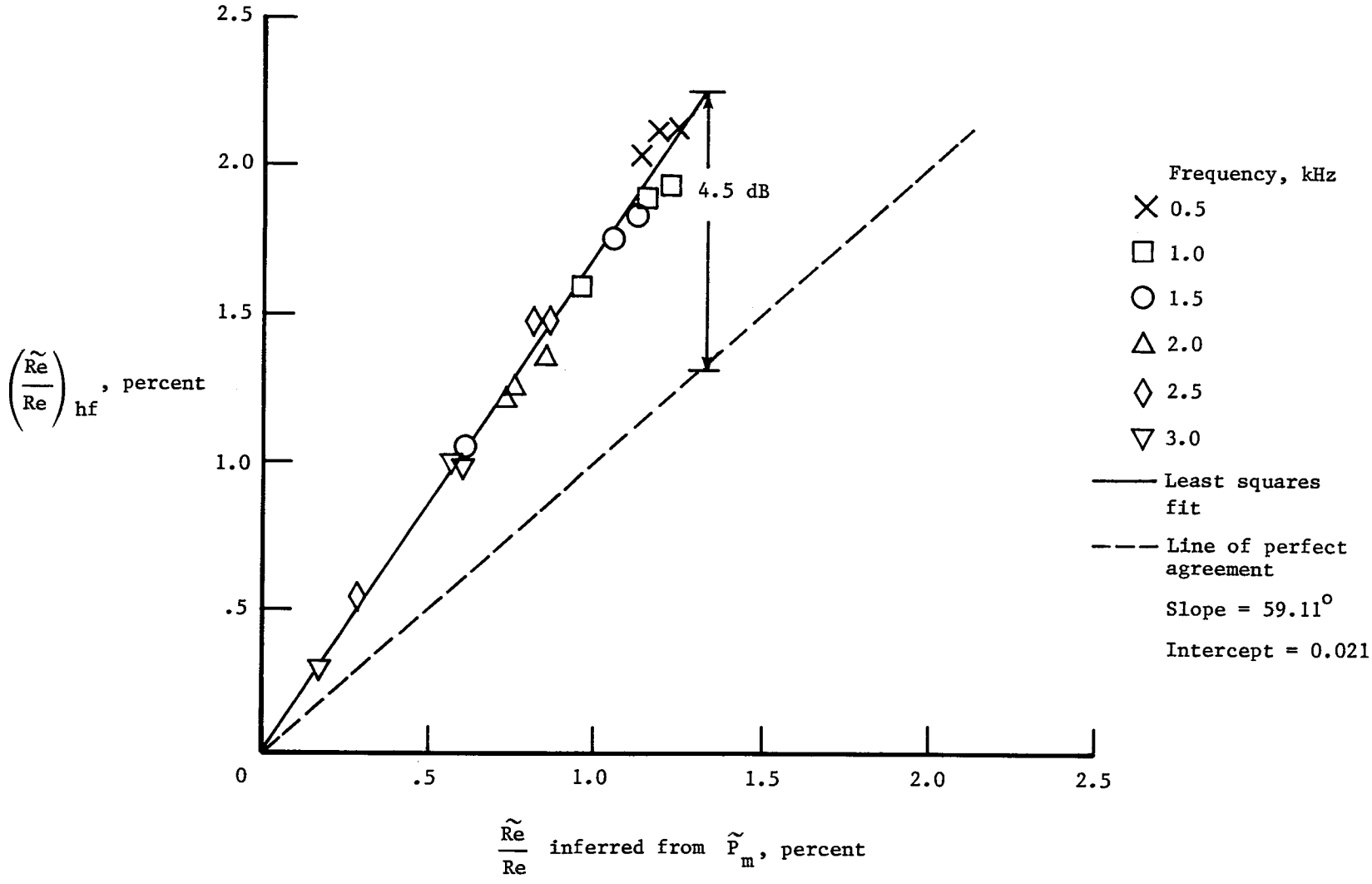

(b) M = 0.3.

Figure 12.- Continued.

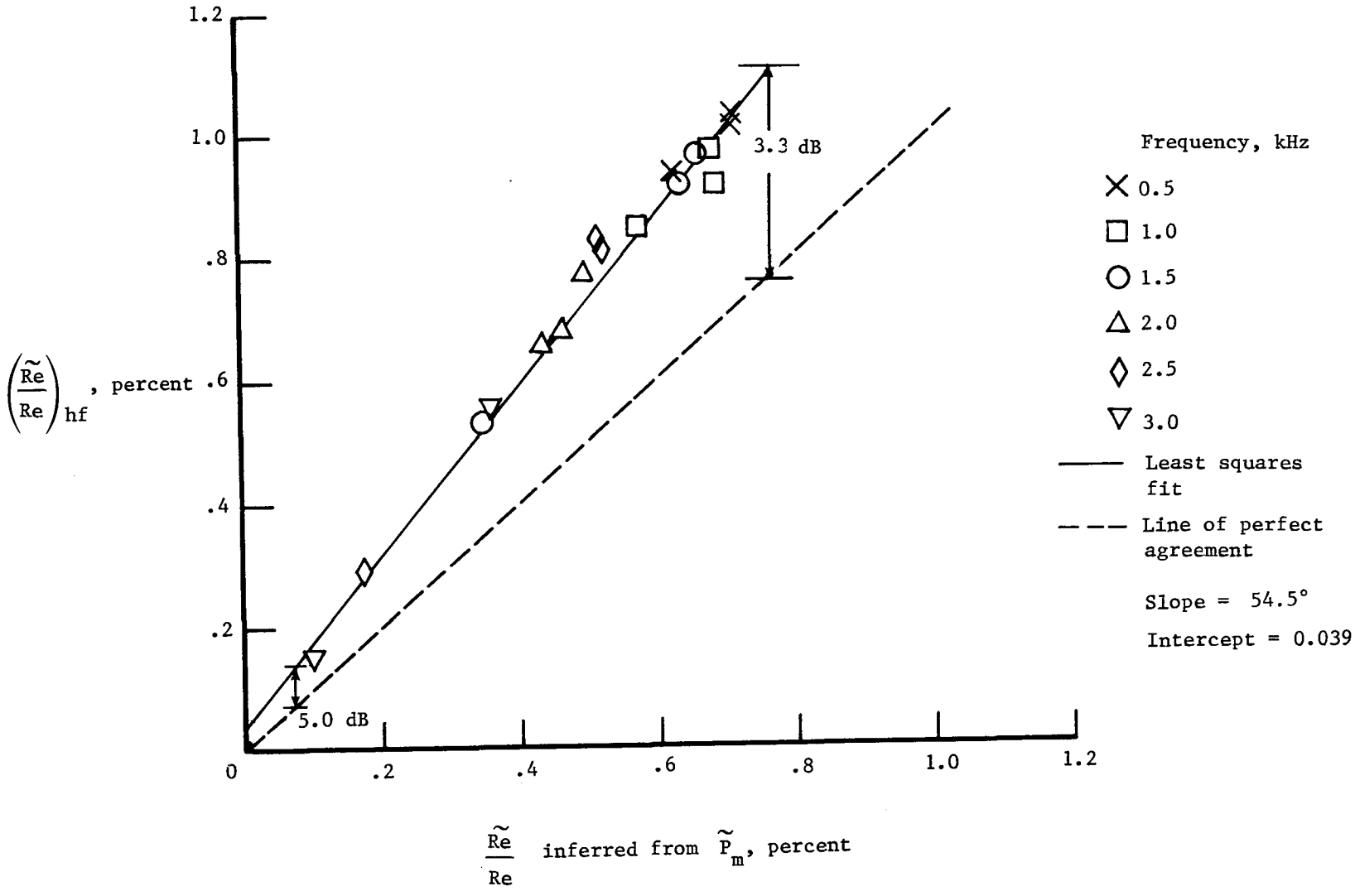

(c) M = 0.5.

Figure 12.- Concluded.

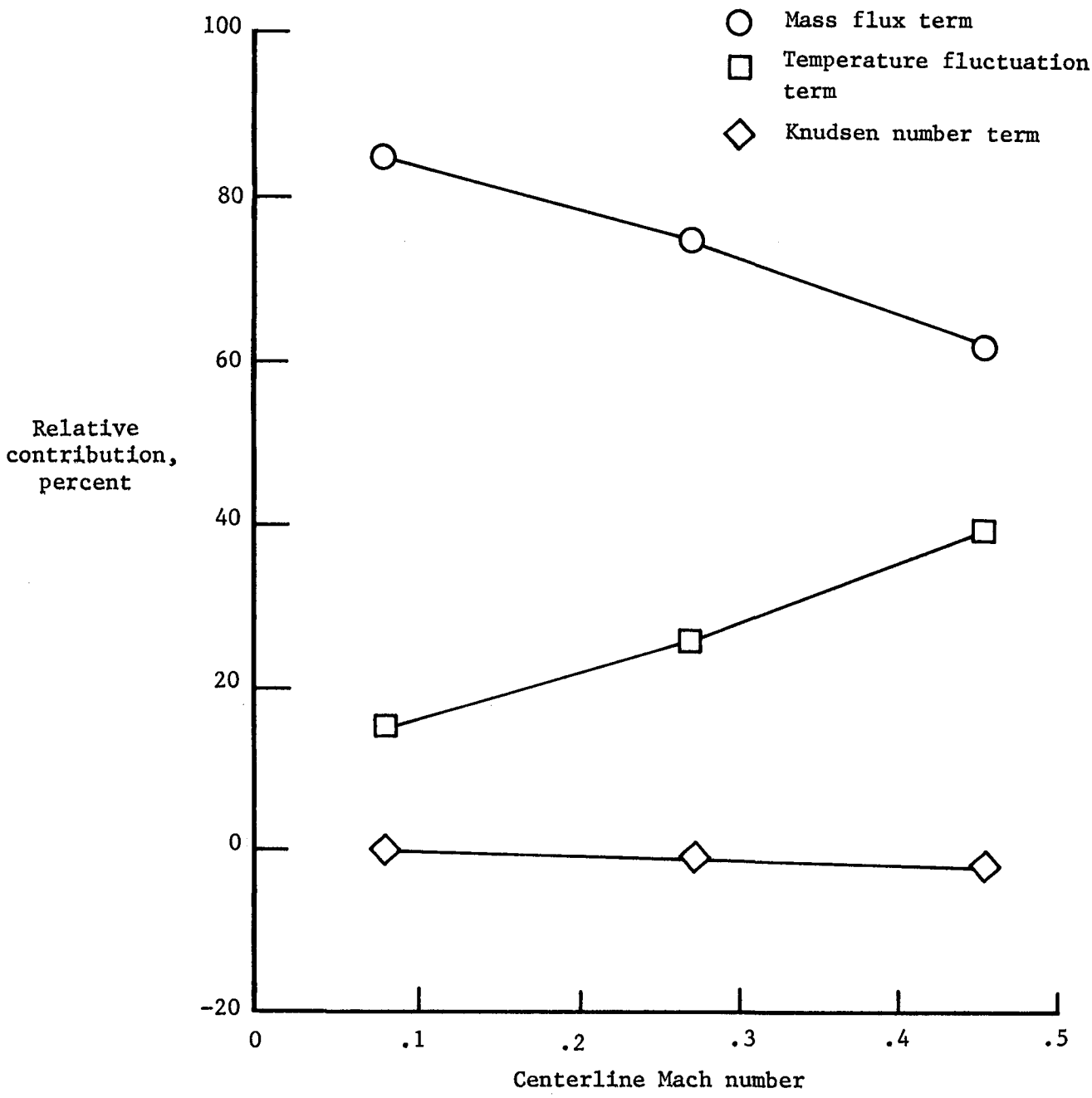

Figure 13.- Relative contributions of terms in equation (27) to $\tilde{Re}/Re$.

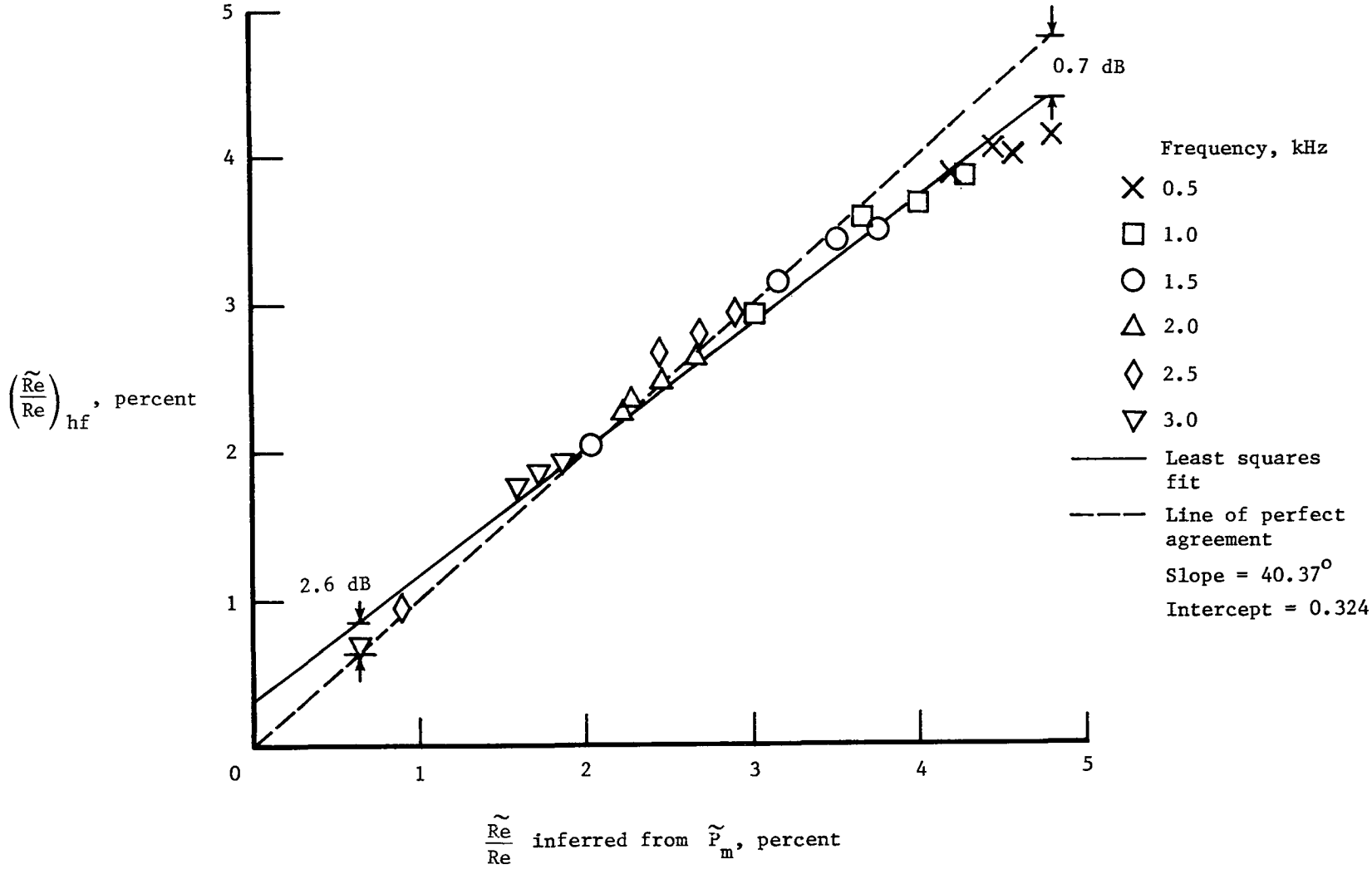

(a) M = 0.1.

Figure 14.- Comparison of hot-film probe and flush-mounted microphone responses (in terms of fluctuating Reynolds number) to acoustic excitation in mean flow (temperature term excluded).

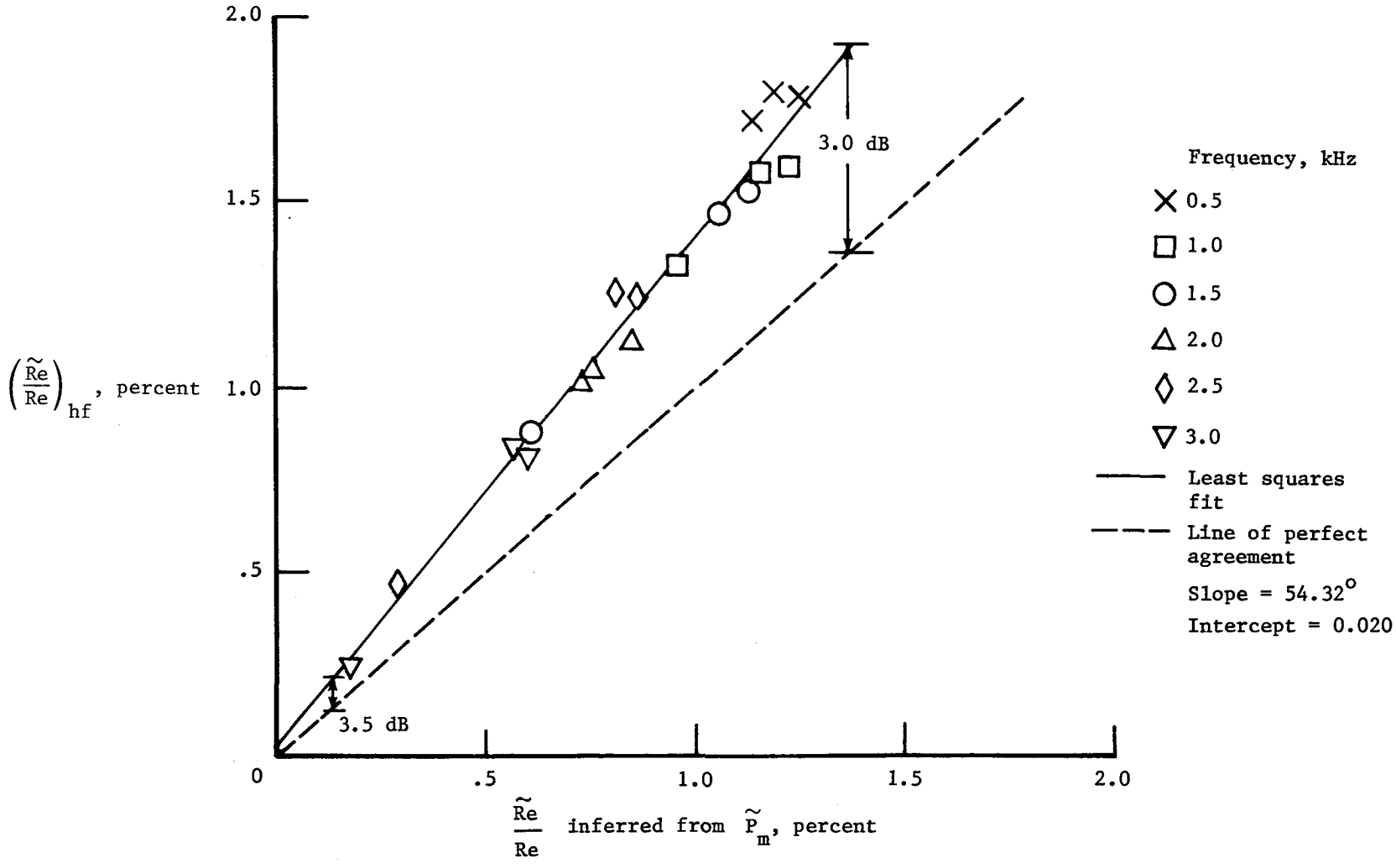

(b) M = 0.3.

Figure 14.- Continued.

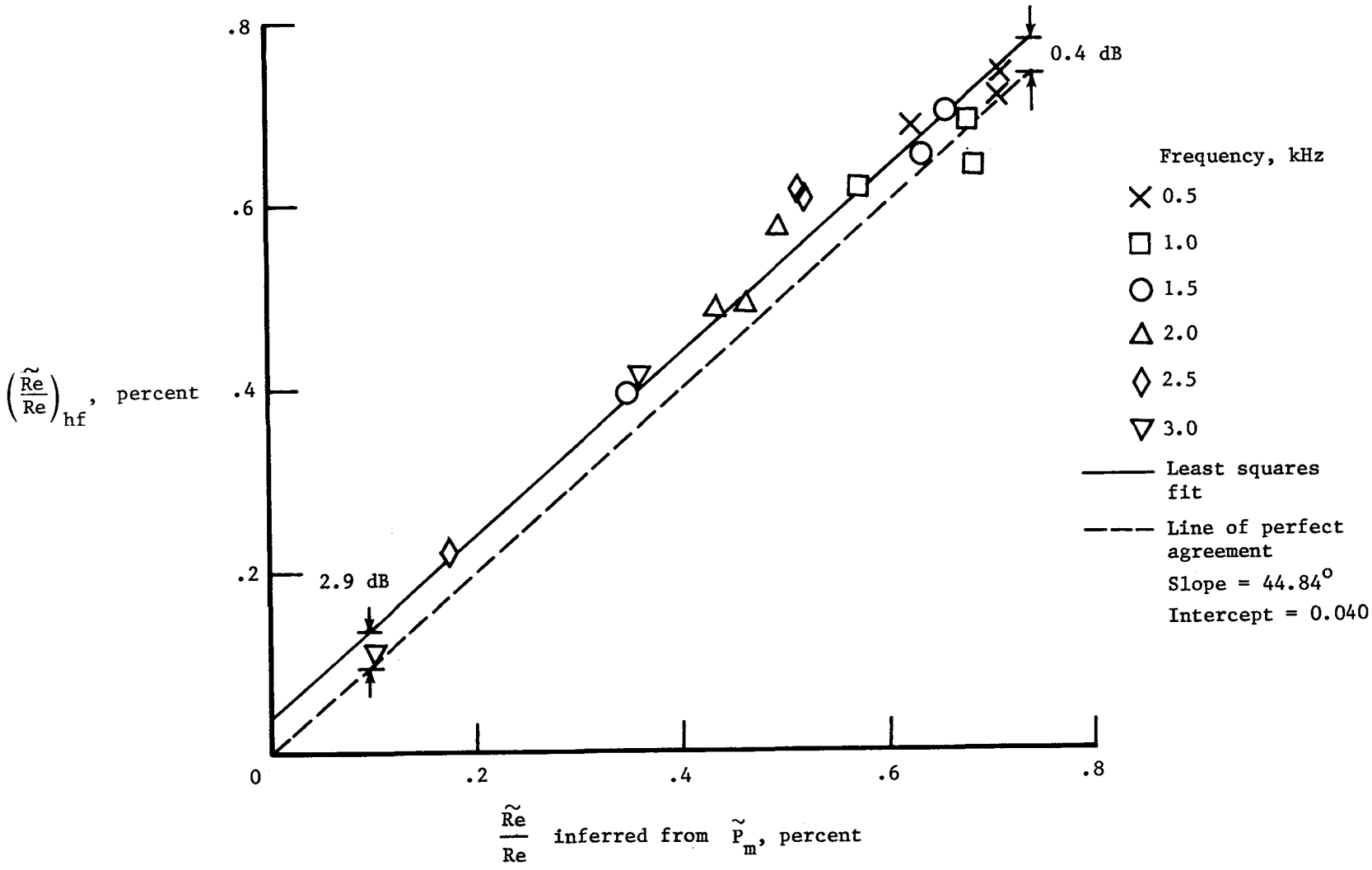

(c) M = 0.5.

Figure 14.- Concluded.

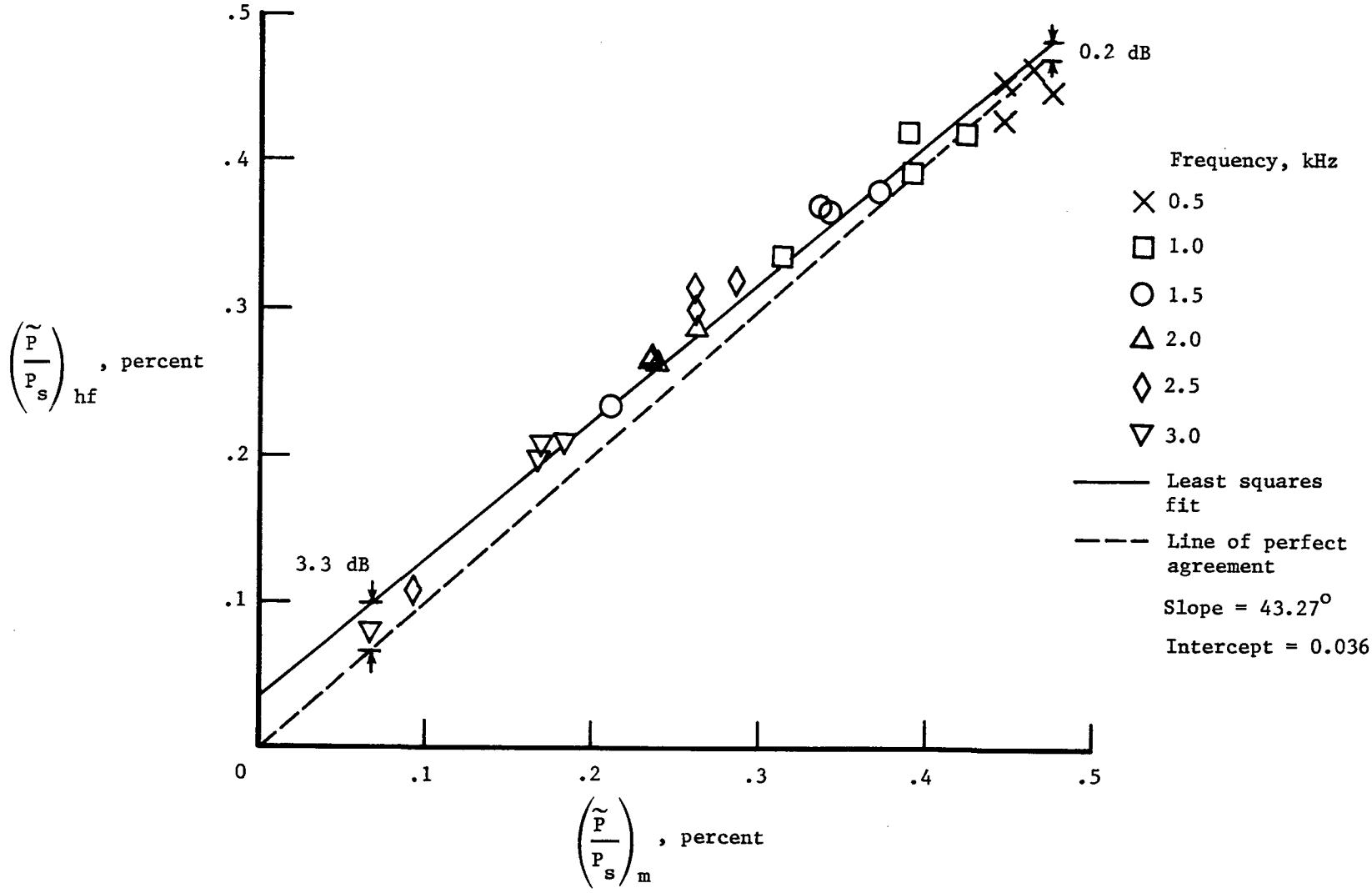

(a) M = 0.1.

Figure 15.- Comparison of hot-film probe and flush-mounted microphone responses (in terms of fluctuating pressure) to acoustic excitation in mean flow.

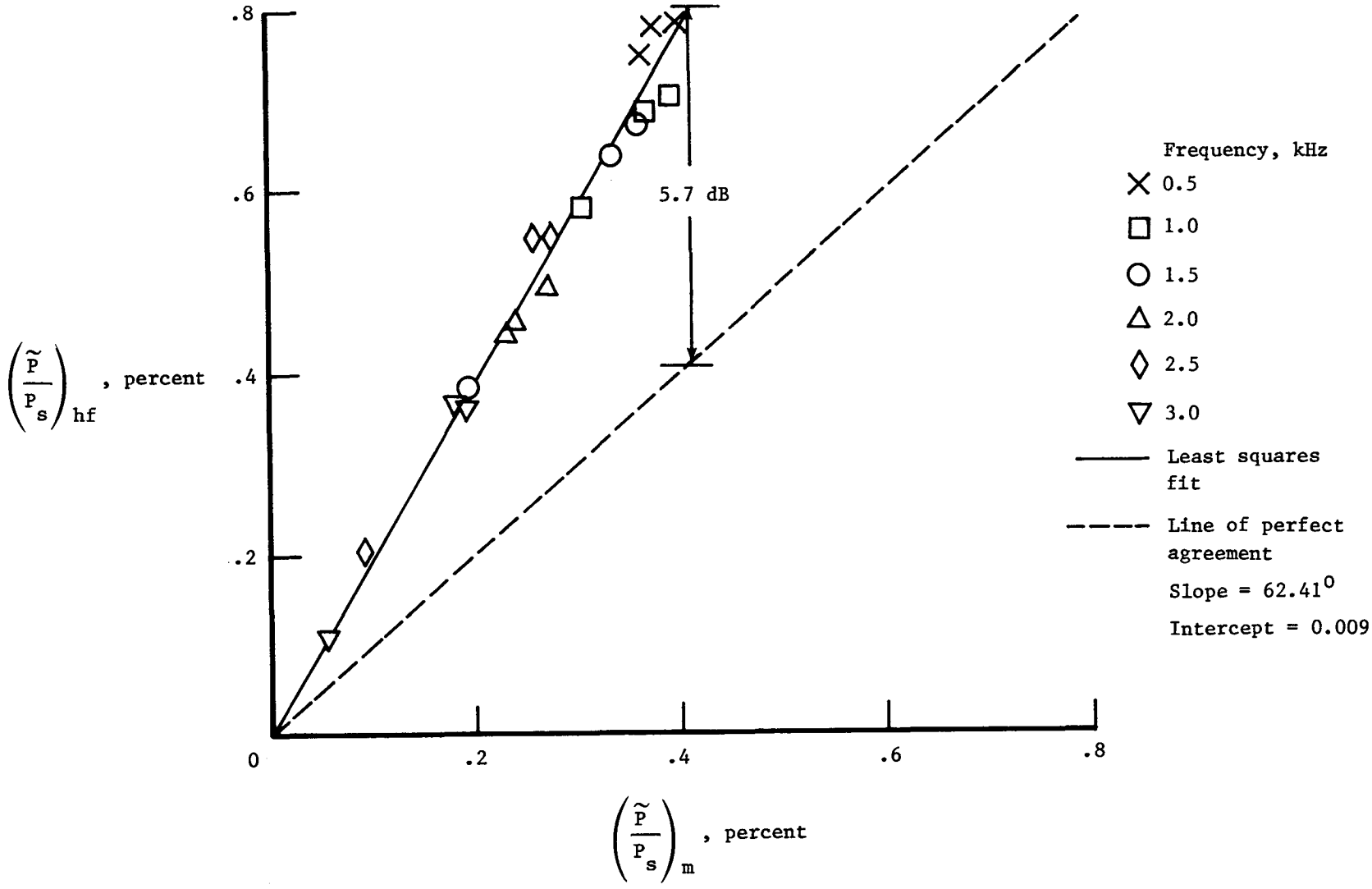

(b) M = 0.3.

Figure 15.- Continued.

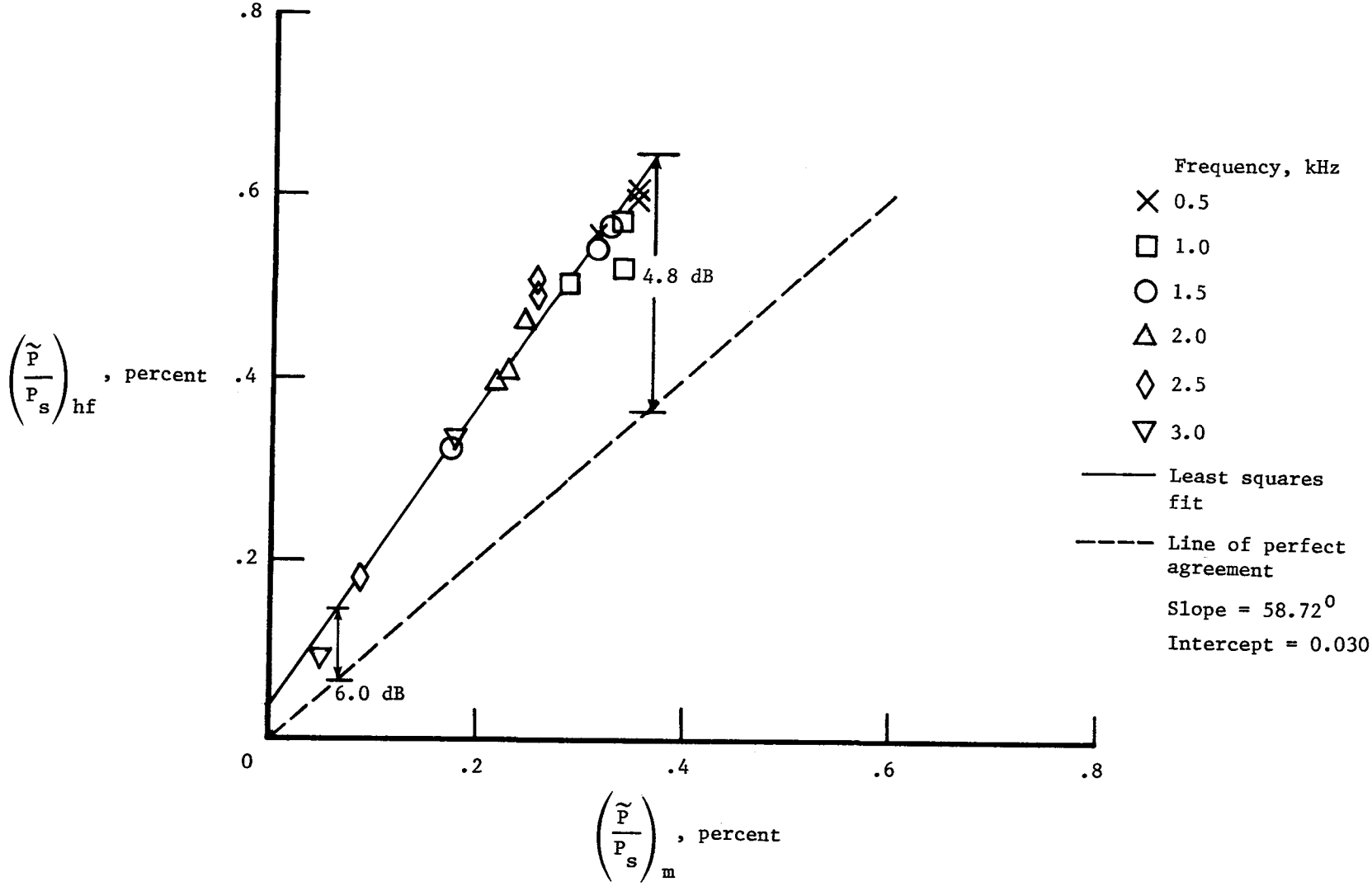

(c) M = 0.5.

Figure 15.- Concluded.

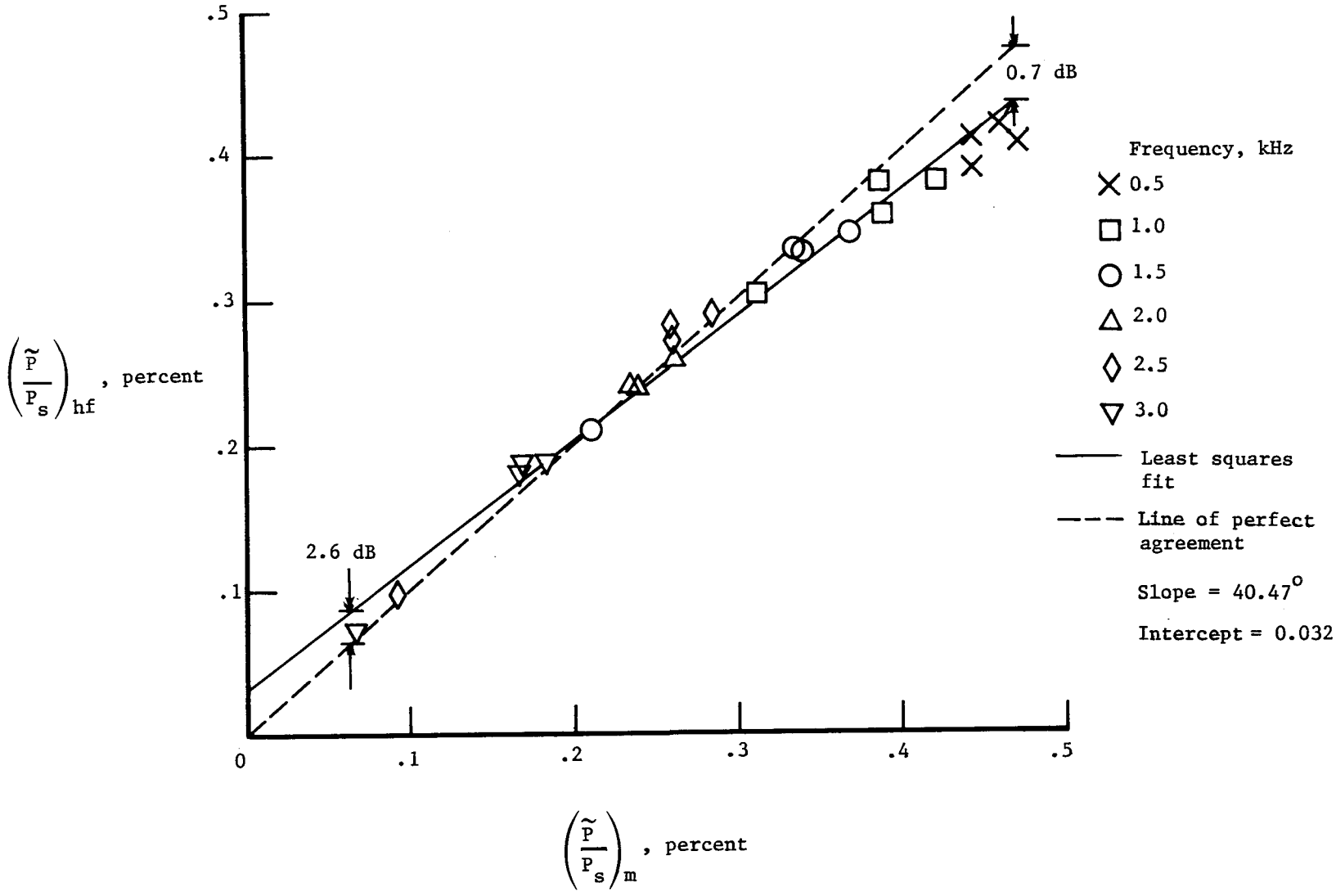

(a) M = 0.1.

Figure 16.- Comparison of hot-film probe and flush-mounted microphone responses (in terms of fluctuating pressure) to acoustic excitation in mean flow (temperature term excluded).

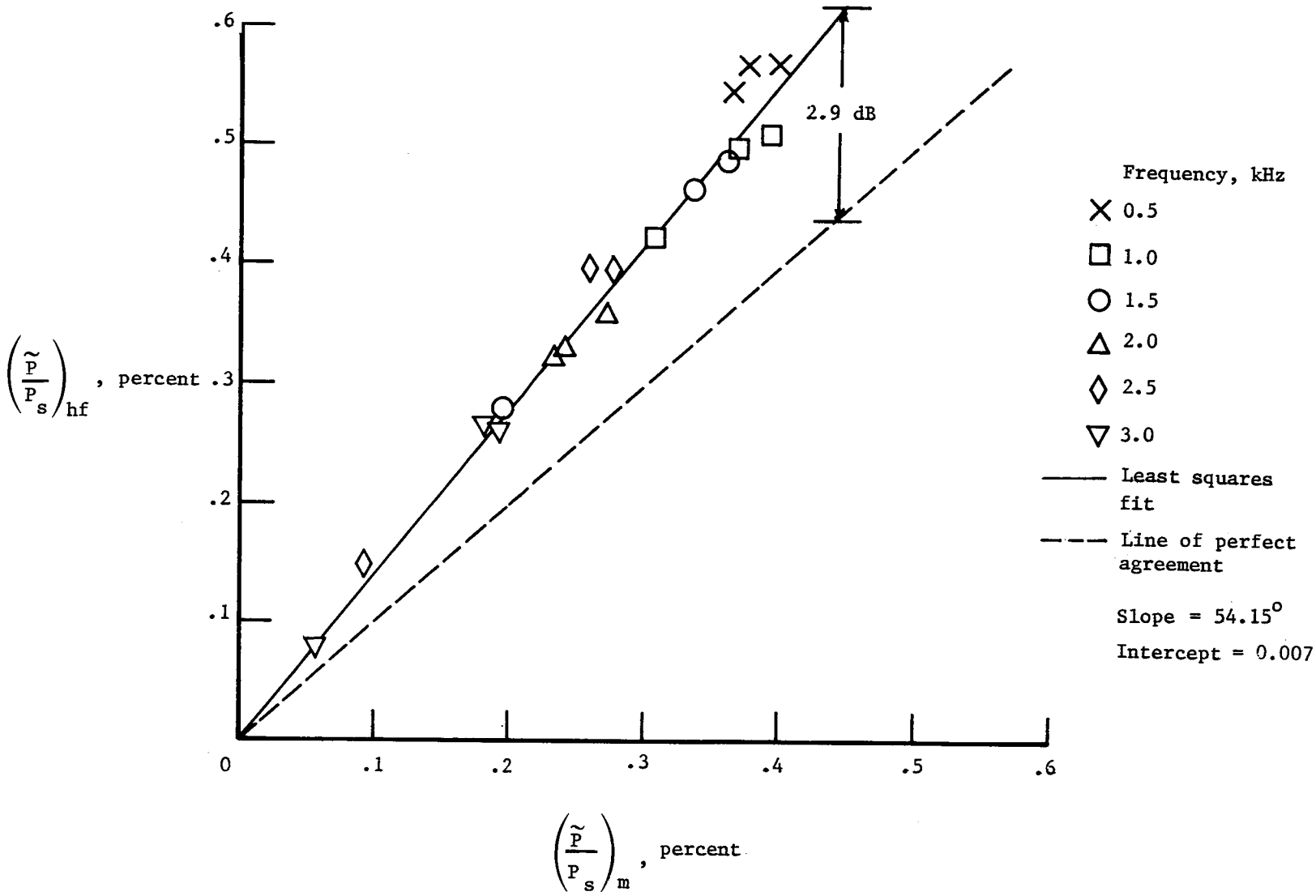

(b) M = 0.3.

Figure 16.- Continued.

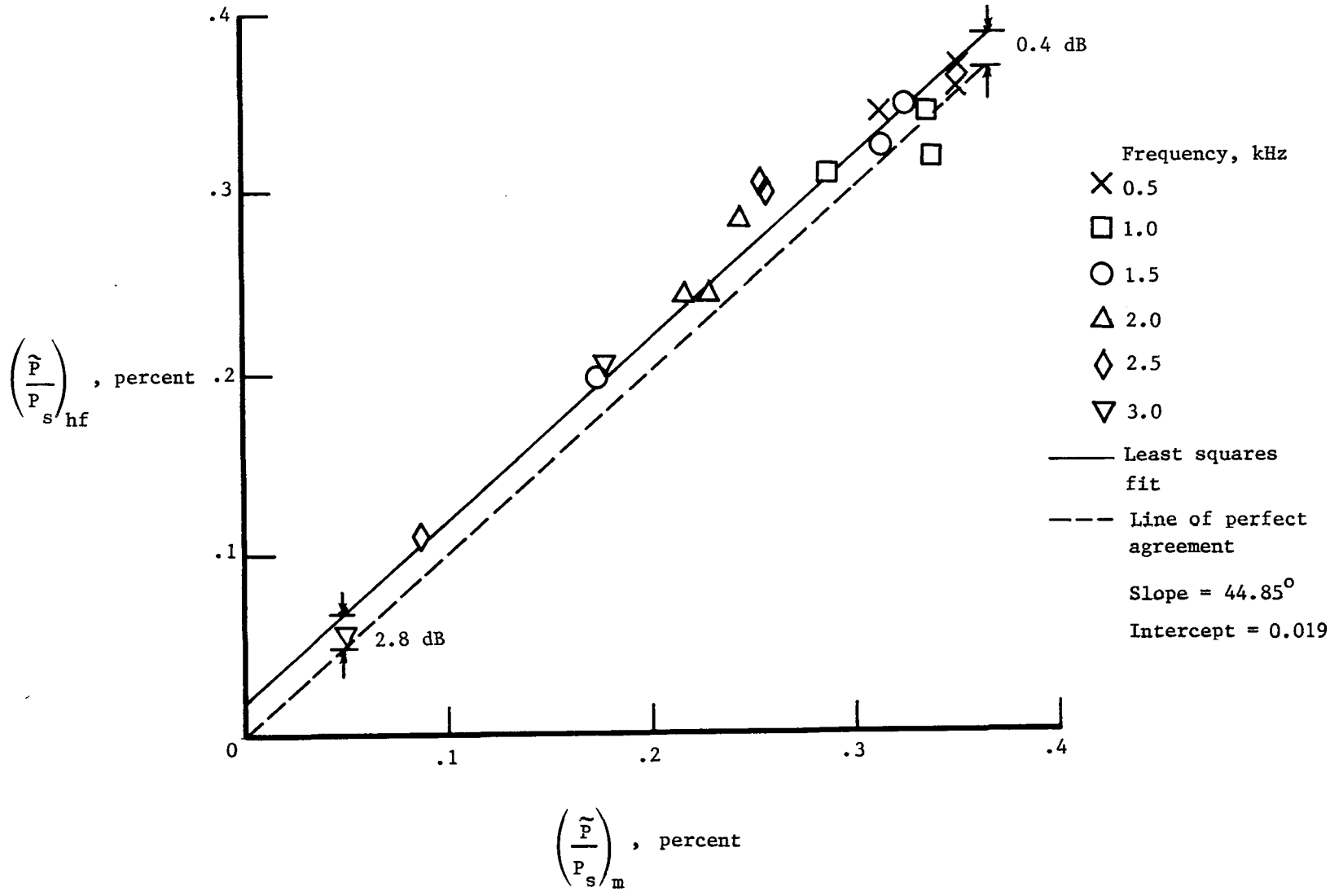

(c) M = 0.5.

Figure 16.- Concluded.

Standard Bibliographic Page

1. Report No.	2. Government Accession No.	3. Recipient's Catalog No.
NASA TP-2581		

4. Title and Subtitle
Pressure Probe and Hot-Film Probe Responses to Acoustic Excitation in Mean Flow

5. Report Date
June 1986

6. Performing Organization Code
505-31-33-13

7. Author(s)
Tony L. Parrott and Michael G. Jones

8. Performing Organization Report No.
L-16079

9. Performing Organization Name and Address
NASA Langley Research Center
Hampton, VA 23665-5225

10. Work Unit No.

11. Contract or Grant No.

12. Sponsoring Agency Name and Address
National Aeronautics and Space Administration
Washington, DC 20546-0001

13. Type of Report and Period Covered
Technical Paper

14. Sponsoring Agency Code

15. Supplementary Notes

Tony L. Parrott: Langley Research Center, Hampton, Virginia.
Michael G. Jones: PRC Kentron, Inc., Hampton, Virginia.

16. Abstract

An experiment was conducted to compare the relative responses of a hot-film probe and a pressure probe positioned in a flow duct carrying mean flow and progressive acoustic waves. The response of each probe was compared with that of a condenser-type microphone flush mounted in the duct wall for flow Mach numbers up to about 0.5. The response of the pressure probe was less than that of the flush-mounted microphone by not more than about 2.1 dB at the highest centerline Mach number. This decreased response of the probe can likely be attributed to flow-induced impedance changes at the probe sensor orifices. The response of the hot-film probe, expressed in terms of fluctuating pressure, was greater than that of the flush-mounted microphone by as much as 6.0 dB at the two higher centerline Mach numbers. Removal of the contribution from fluctuating temperature in the hot-film analytical model greatly improved the agreement between the two transducer responses.

17. Key Words (Suggested by Authors(s))	18. Distribution Statement
Steady flow Acoustic measurement Hot-film probes Pressure probes Fluctuating pressure Fluctuating Reynolds number	Unclassified - Unlimited Subject Category 71

19. Security Classif.(of this report)	20. Security Classif.(of this page)	21. No. of Pages	22. Price
Unclassified	Unclassified	54	A04

For sale by the National Technical Information Service, Springfield, Virginia 22161

NASA-Langley, 1986

National Aeronautics and
Space Administration
Code NIT-4

Washington, D.C.
20546-0001